Expertise
and insight
for the future

Antti Nurminen

# Photodetector Amplifier and Measurement Setup Design

Metropolia University of Applied Sciences

Bachelor of Engineering

Degree Programme in Electronics

Bachelor's Thesis

13 January 2021

| | |
|---|---|
| Author<br>Title<br><br>Number of Pages<br>Date | Antti Nurminen<br>Photodetector Amplifier and Measurement Setup Design<br><br>50 pages + 4 appendices<br>13 January 2021 |
| Degree | Bachelor of Engineering |
| Degree Programme | Electrical and automation engineering |
| Professional Major | Electronics |
| Instructors | Tapio Pernu, Research Team Leader<br>Matti Fischer, Principal Lecturer |

This thesis work was conducted at VTT Technical Research Centre of Finland Ltd. with the goal of creating a measurement setup for a novel nanotechnology-based photodetector. Photodetectors are widely used for example in imaging, motion detection, and biomedical applications. Research and development of electronic components require measurements, which can be used to characterize the component.

A measurement setup and an accompanying amplifiers for the photodetector were designed, constructed, and verified. Two testboard PCBs were designed using PADS software: The mainboard, which amplifies the signal, and the daughterboard, which houses the photodetector. The testboards were fixed to the measurement setup with a TMc300 Monochromator, which is used to provide a calibrated bandwidth of incident light. This system achieves the measurement of the signal with different bias voltages and lighting conditions. Automation of the measurement and data acquisition was done using a LabVIEW program.

The photodetector to be characterized was not yet manufactured, therefore the performance of the testboards was verified with a current source. The complete measurement setup was also verified with ready-made phototransistors used as reference. The results showed the measurement setup to be suitable for photodetector characterization measurements, and the implemented amplifiers were verified to be able to accurately measure small signal currents.

| | |
|---|---|
| Keywords | Photodetectors, Photodiodes, Optical Sensor, Amplifier, Measurement Setup |

| | |
|---|---|
| Tekijä<br>Otsikko<br><br>Sivumäärä<br>Aika | Antti Nurminen<br>Valoanturin vahvistimen ja mittausalustan suunnittelu<br><br>50 sivua + 4 liitettä<br>13.1.2021 |
| Tutkinto | insinööri (AMK) |
| Tutkinto-ohjelma | sähkö- ja automaatiotekniikka |
| Ammatillinen pääaine | elektroniikka |
| Ohjaajat | tutkimustiimin päällikkö Tapio Pernu<br>yliopettaja Matti Fischer |

Insinöörityö tehtiin Teknologian tutkimuskeskus VTT Oy:lle. Työn tarkoituksena oli mittausalustan suunnittelu uudentyyppiselle nanoteknologiaan perustuvalle valoanturille. Valoantureita käytetään laajasti esimerkiksi kuvantamiseen, liiketunnistukseen ja lääketieteen sovelluksiin. Uusien komponenttien tutkimus ja tuotekehitys vaatii mittauksia, joiden avulla voidaan karakterisoida kyseinen komponentti.

Anturin tutkimista varten suunniteltiin, toteutettiin, ja verifioitiin vahvistimet ja mittausalusta. Anturille suunniteltiin kaksi piirilevyä PADS-ohjelmistolla: pääkortti, joka vahvistaa anturin signaalin, ja tytärkortti, johon anturi on asennettu. Ne kiinnitettiin mittausalustaan kuuluvan TMc300-monokromaattorin ulostuloon, joka antaa kalibroidun valokaistan anturille. Tällä järjestelyllä voidaan mitata valoanturia eri käyttöjännitteillä ja eri valaistuksissa. Mittaukset automatisoitiin ja tulokset kerättiin LabVIEW-ohjelmalla.

Uusi valoanturi ei ollut vielä valmistunut, joten vahvistimien toimivuus verifioitiin virtalähteen avulla. Mittausalusta kokonaisuudessaan verifioitiin käyttäen olemassa olevia fototransistoreita vertailukohteena. Tulokset osoittivat mittausalustan olevan käyttökelpoinen valoanturien karaterisointiin, ja vahvistimilla pystytään mittaamaan pieniä virtoja hyvällä tarkkuudella.

| | |
|---|---|
| Avainsanat | valoilmaisin, fotodiodi, optinen sensori, vahvistin, mittausjärjestely |

## Contents

## List of Abbreviations

| | |
|---|---|
| AN | Anode |
| CA | Cathode |
| CMRR | Common Mode Rejection Ratio |
| EMC | Electromagnetic |
| EXT | External |
| INT | Internal |
| IV-C | Current-to-Voltage Converter |
| LDR | Light-Dependent Resistor |
| OP AMP | Operation Amplifier |
| PCB | Printed Circuit Board |
| PSRR | Power Supply Rejection Ratio |
| SNR | Signal-to-Noise ratio |
| TIA | Transimpedance amplifier |
| VTT | Technical Research Centre of Finland |

# 1 Introduction

Photodetectors are fundamental to the field of photonics, and they are widely used for measuring electromagnetic radiation. They have a broad range of applications in many technology sectors. Modern optical sensors mainly use semiconductor components based on the photoelectric effect. VTT Technical research centre of Finland, hereafter VTT, provides research and innovation in semiconductors, sensor technology, and in many other fields. Reliable and accurate measurements are required in research and development of photodetectors and other electronics.

The goal of this thesis was to design and implement a measurement setup, and an amplifier for a novel nanotechnology-based photodetector developed at VTT, so it could be characterized after it is manufactured. The details of the photodetector are confidential. It is treated as a typical p-n junction photodiode in this thesis, as from the electronics point of view the behavior is identical. Thus, it does not affect the measurement setup or amplifier design.

The measurement setup was designed by examining the properties of existing equipment and combining them into a working measurement system. Amplifiers for the photodetector device were designed in PADS PCB Design Software. The circuit boards were designed to be compatible with both the photodetector and the measurement setup. The design process involved a literature review of properties and circuits of op amps to accomplish an amplifier with low noise, and a good accuracy and precision. Measurements were made to verify the performance of the amplifiers and the measurement setup.

# 2 Theoretical Background

## 2.1 Semiconductors

Most of modern technology relies on semiconductor devices. Their properties enable the manufacturing of nanosized electrical components, utilized for example in

microprocessors or in other integrated circuits. Semiconductors have been, and still are, a subject of extensive research and development both in the academia and in the industry. [1,7-10.]

Many different semiconductor materials exist, three most important being silicon (Si), germanium (Ge), and gallium arsenide (GaAs). The property that all semiconductors share is that their conductivity is between conductors and insulators. The electrical properties of these materials can be easily and significantly altered by intentionally introducing impurities and imperfections, with varying materials and techniques. This is called doping. [2,1-23.]

Typically, semiconductors are doped crystalline solids, where the atoms are arranged in a repeating pattern, called crystal lattice. This pattern is based on how the atoms interact with neighboring atoms. For an example, the most used semiconductor, silicon, has a diamond lattice structure, where each Si-atom has a covalent bond with its four nearest neighbors. In this structure there is no conductivity, as all the mobile electrons are in a bonded state, so in its pure form Si is a nearly perfect insulator. [1,8-11; 3,1-7.]

### 2.1.1 Band Gap

Atom's electrons have quantized energies, and because of the Pauli exclusion principle, electrons cannot occupy the same physical state with one another. This results in electron shells, subshells, and orbitals in an atom, where electrons have different energies, angular momentums and spins. [4.]

Generally, the atomic orbitals are filled from the lowest energy upwards with electrons, according to the Aufbau rule. The highest almost filled electron shell is called the valence band, and the lowest almost empty electron shell is called the conduction band. Both of these bands determine the electrical conductivity of the material, since the electrons can move in both bands. The gap in between these bands is called the band gap, and the difference between the electron energy levels in these bands is called band gap energy or energy gap. This is the energy required to move one electron from the valence band to the conduction band. [3,8-11.]

### 2.1.2 Doping

Doping is the process of introducing impurity atoms to a semiconductor material. It is done to modify the properties of the material. Semiconductors are often doped to have more or less charge carriers than their pure form would have, to make them more conductive. The net charge of the material stays neutral, but the conductivity changes. The band gap can be adjusted to a desired value through doping with a certain concentration of dopant atoms. [3,10-12.]

Semiconductors that have been doped with 'donor'-impurities, which are atoms that bring more mobile electrons to the material, are called n-type semiconductors. For example, silicon can be doped with arsenide, which has five valence electrons, four of them are shared with neighboring silicon atoms, and one electron is left free to carry charge. [3,10-12;5,636-638.]

Similarly, a semiconductor can be doped with 'acceptors', which are atoms that can bond more electrons than surrounding semiconductor atoms. The absence of an electron leaves a hole in the valence band which is essentially a positive charge carrier. This type of doped semiconductor is called a p-type. Doped semiconductors are referred to as extrinsic materials, and undoped are called intrinsic materials. [3,10-12;5,636-638.]

### 2.1.3 P-N Junction

Most modern electronic devices that are based on semiconductor technology utilize the properties of a p-n junction, which is the boundary between a p-type and an n-type doped semiconductor regions. A typical diode is essentially just a p-n junction.

When a piece of semiconductor is doped to a p-type on one side, and an n-type on the opposite, the conductive electrons in the n-type are attracted towards the holes on the p-type. The electrons and holes are diffused together in both sides near the junction as can be seen in Figure 1. [2,238-250.]

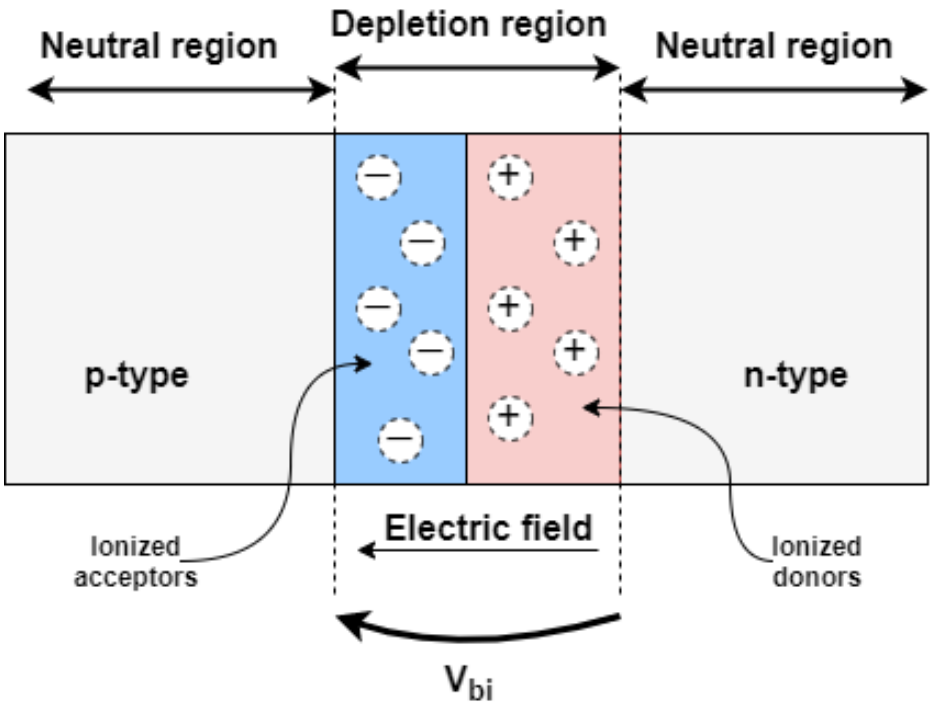


Figure 1. An unbiased p-n junction (reproduced from [2,239]).

This diffusion of charge carriers results in an isolating neutral region, called the depletion region, at the junction, as seen in Figure 1. This leaves positively charged donor atoms on the n-region, and negative acceptor atoms on the p-region, at the sides of the junction. These charges induce an electric field from the n-region to the p-region across the depletion region, which prevents the electrons and holes diffusing further. The potential difference from this electric field is referred to as built-in voltage, denoted by $V_{bi}$. [5,650-653.]

In the case that a forward bias voltage is applied across the p-n junction, so that the p-type is at a higher potential than n-type, the charge carriers at the junction will be influenced. If the external voltage is high enough to overcome the built-in voltage, the bias lowers the potential barrier for charge carriers to move through the junction, so it becomes conductive and a current would flow through the diode. [5,651-653; 6,67-75.]

In the case of negative bias voltage across the p-n junction, the external voltage contributes to the built-in voltage at the junction, increasing the potential barrier. The increased electric field pulls the charge carriers further apart, also decreasing the junction

capacitance caused by the increased depletion region width, a property which is used in voltage-variable capacitors. In this case only a very small leakage current flows through the component, called the reverse saturation current, caused by the diffusion of the carriers. These behaviors give rise to the I-V characteristics of a p-n junction diode, shown in Figure 2. [2,247-250; 6,73-75.]

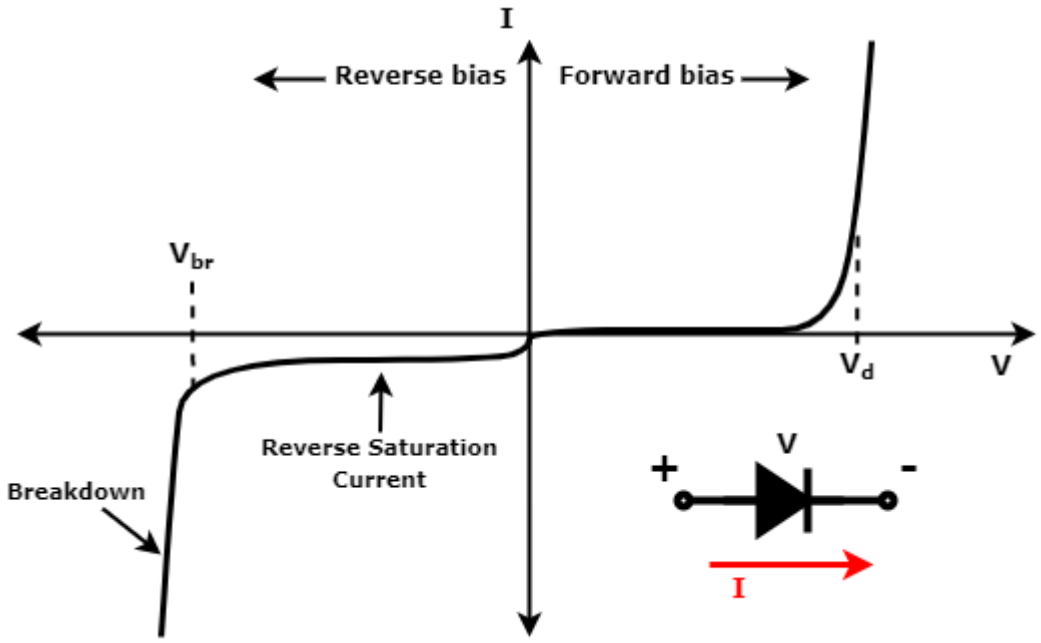


Figure 2. I-V characteristic of a typical diode (reproduced from [6,78]).

In Figure 2, $V_d$ refers to the threshold voltage of the diode and $V_{br}$ is the voltage level in which the diode breaks. This diode model ignores thermodynamics and quantum tunneling of charges, but it represents the basic functionality accurately. [6,74.]

## 2.2 Photoelectric Effect

Photosensors usually convert photons into a measurable form through the photoelectric effect phenomenon. The basic principle is that a photon has energy, which is proportional to its wavelength as in equation 1. [3,9-10.]

$$E = \mathrm{hf} = \frac{\mathrm{hc}}{\lambda} \quad (1)$$

Where E is the energy of the photon, h is the Planck's constant, f is the frequency of the photon, c is the speed of light, and λ is the light's wavelength. If this energy is sufficient, meaning the wavelength is short enough, the photon can excite an electron of an atom in the material, which results to increased energy state of the electron. The electrons have discrete energies, so they can be elevated to a higher band, and the leftover energy of the photon is exhibited as the kinetic energy of the excited electron. If the energy of the photon is high enough, the electron can also completely escape the material, and ionize the atom. Both cases are illustrated in Figure 3. [5,660-669; 6,303-305.]

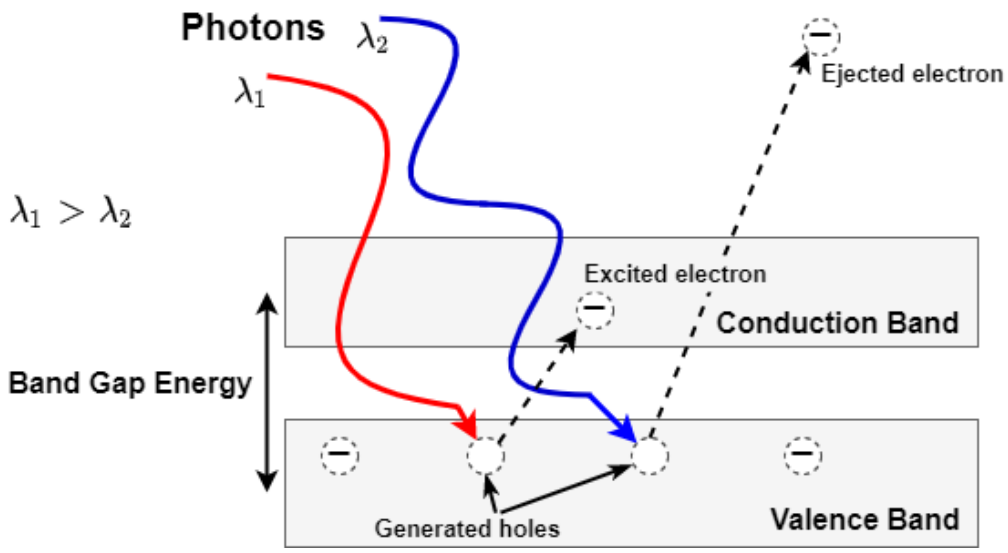


Figure 3. Photoelectric Effect (reproduced from [2,619]).

Photoelectric effect happens due to the absorption of a photon, which is called the photoelectron emission. It is most likely to happen in the bands where the electrons are plentiful, in metals this would be conduction band, and in intrinsic semiconductors the valence band. Since there are newly created free charge carriers, the materials conductivity rises, this response is referred to as photoconductivity. [1,743-754].

In most semiconductor photodetectors this photoelectric effect happens internally in the depletion region, so that the excited electron stays in the sample. The photon essentially separates the negative and positive charge carriers across the band gap. This separation is called electron-hole photogeneration. The positive and negative charge carriers would then move in the opposite directions under the internal electric field and would generate a current referred to as photocurrent. The afore mentioned reverse saturation current is

referred to as dark current in p-n junction-based detectors, and more generally dark current refers to the current through the photodetector component when it is not exposed to light. [5, 660-669, 751-752.]

## 2.3 Photodetector Components

Basic electronical components used in photosensors are photodiode, phototransistor, and LDR (light-dependent resistor). Examples of these components are shown in Figure 4.

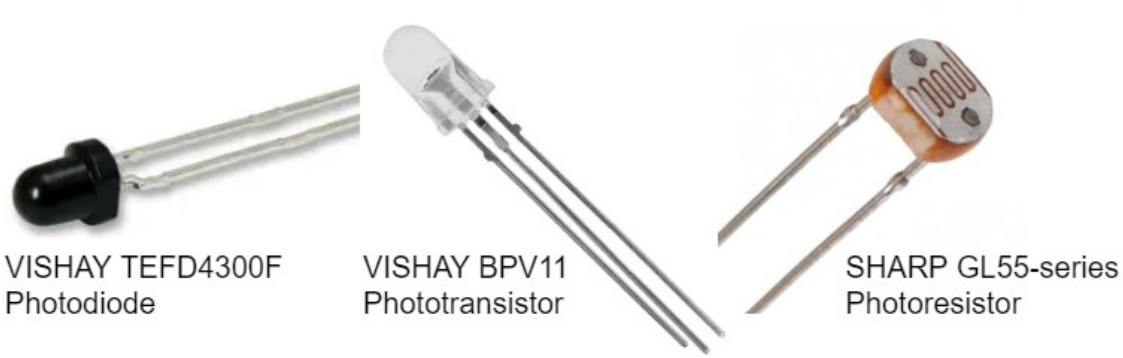


Figure 4. Photodetector components [7;8;9].

These are available in many different packages, as are other electronic components.

### 2.3.1 Photodiodes

A basic photodiode is a simple p-n junction diode made from photosensitive material, with the junction exposed for incoming light. The photoelectric effect takes place when a photon hits an atom in the junction, with greater energy than the band gap energy. Hence photosensitive materials have band gap energies corresponding to the values of wavelengths they are sensitive to. [10; 11.]

Photodiodes can be used in two different modes, photovoltaic and photoconductive, corresponding to different biases. Figure 5 shows the behavior of a photodiode with different biases in different lighting conditions.

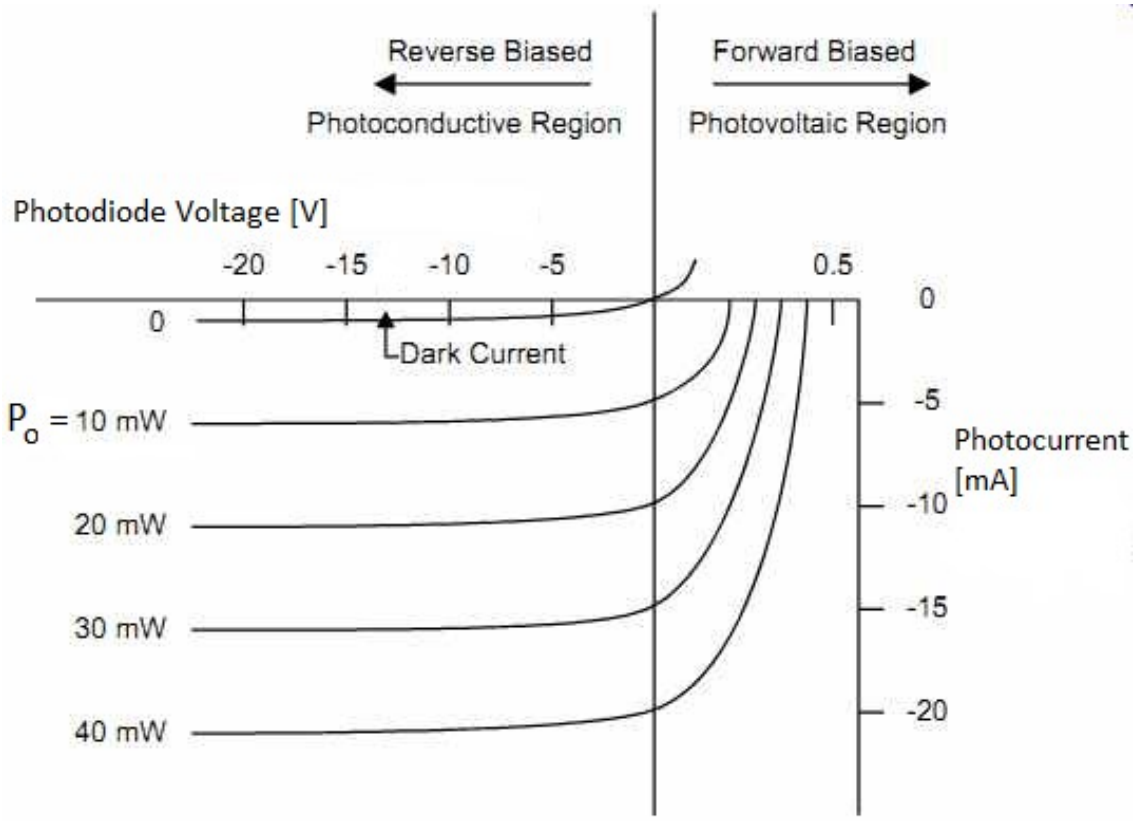


Figure 5. Example of an I-V curve of a photodiode [12].

In photovoltaic mode, the diode is zero biased, and the light generates a voltage due to photogeneration. However, output voltage in this mode is not linear with optical power $P_o$, and the dynamic range is small, as can be seen from Figure 5, but the dark current is minimized. In photoconductive mode a negative bias is applied, providing a current which is sufficiently linear with optical power over six or more orders of magnitude. The amount of negative bias voltage does not affect the photocurrent magnitude significantly, as it is sourced by the incident light. Higher reverse bias voltages usually decrease the response time, but also contributes to the heating of the diode. [10;11.]

A photodiode can be modeled with an equivalent circuit shown in Figure 6.

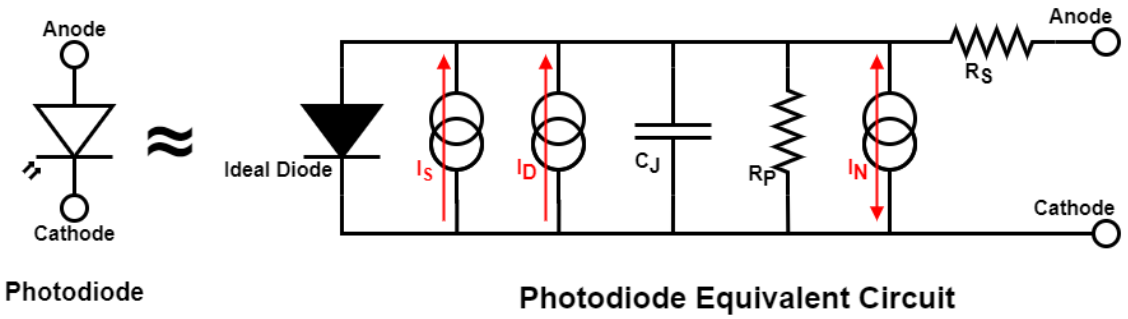


Figure 6. Photodiode equivalent circuit (reproduced from [10]).

The photocurrent in the equivalent circuit is represented as a current source $I_s$, parallel to it, there is a noise current $I_N$, and a small dark current $I_D$ coming from randomly generated electron-hole pairs, which are not due to external light, but mainly from thermal ambiance. Capacitance of the p-n junction is $C_J$, which can vary with the applied bias voltage. An ideal diode is included, which provides the characteristic I-V curve behavior. Additionally, a large parallel resistance $R_P$ and a small serial resistance $R_S$ exist in real world components. [10;11.]

The photocurrent $I_s$ and responsivity R for a specified wavelength are related through equation 2.

$$I_s(\lambda) = \mathrm{R}(\lambda) * \mathrm{P_o}(\lambda) \tag{2}$$

Where $P_o$ is the optical power on the active area of the photodiode. The responsivity for a specified wavelength $\lambda_o$ is defined in the equation 3.

$$\mathrm{R}(\lambda_o) = \frac{\eta\,(\lambda_o) * e}{\mathrm{hf}} \approx \eta\,(\lambda_o)\frac{\lambda_o}{1.24} \tag{3}$$

In this equation, e is the elementary charge, f is the light's frequency, and η is the quantum efficiency for the specified wavelength. Quantum efficiency is simply the probability of a single photon to produce a carrier pair, which contributes to the photocurrent. [5,753-754.]

Along with responsivity, the active light sensitive area is important with photodiodes. Bigger area offers more charge carriers to be photogenerated. Photodiodes are often made

as PIN diodes, where there is an intrinsic, undoped layer between the p- and n-regions which expands the photosensitive depletion region. This increases the active area of the component, and it also decreases the junction capacitance. The junction capacitance combined with the serial resistance in the equivalent circuit form a low pass filter, the time constant associated with these limits the time response of the component, which should be considered when adding external components. [2,267-279; 5,653.]

Even with good efficiency, the thermal noise and shot noise limit the detectable illumination levels. In semiconductor devices the fluctuations in the electron-hole pair generation also produce a significant noise, called generation-recombination noise, or g-r noise. [6,318-319.]

Photocurrent can be more isolated from the different effects in the component if a measurement is taken in the same conditions without the light stimulus. This can be done by covering the light source or the detector in-between measurements, this is referred to as dark measurement. [13.]

### 2.3.2 Phototransistors

Phototransistors are essentially bipolar junction transistors, where the base-collector junction is exposed to light. The p-n junction in the base-collector works like a photodiode, but the current is internally amplified. The symbol for a phototransistor, along with the equivalent circuit is shown in Figure 7. [6,341-343.]

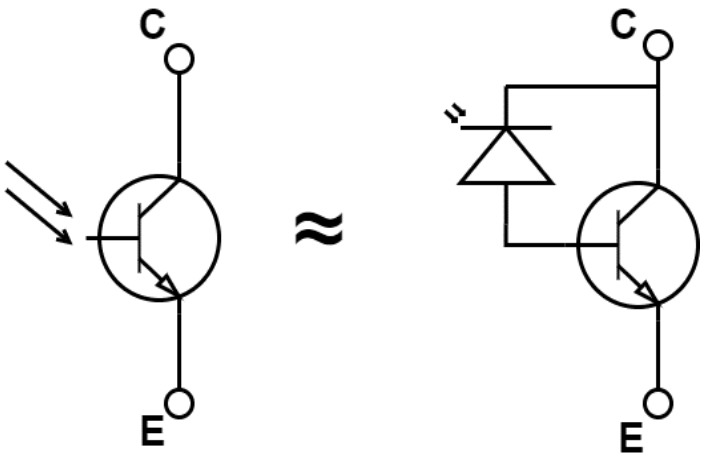


Figure 7. Phototransistor equivalent circuit (reproduced from [6,341]).

The base of the transistor is left unconnected, as seen in Figure 7, it only receives the incoming photons as in a photodiode. The photons create the photocurrent in the base, which is then amplified by the transistors internal gain. [6,341-343.]

The advantage of phototransistor compared to photodiode is that the internal gain simplifies the external circuitry. However, the internal gain affects also the dark current, so it cannot detect dimmer light levels, and the larger junction capacitance results in a small bandwidth of a few hundred kilohertz. [6,341-343;14.]

### 2.3.3 Photoresistor

Photoresistors are also known as light-dependent resistors, photo-conductive cells, and photoconductors. They are commonly referred to as LDR, for light dependent resistance. Photoresistor symbol is shown below in Figure 8.

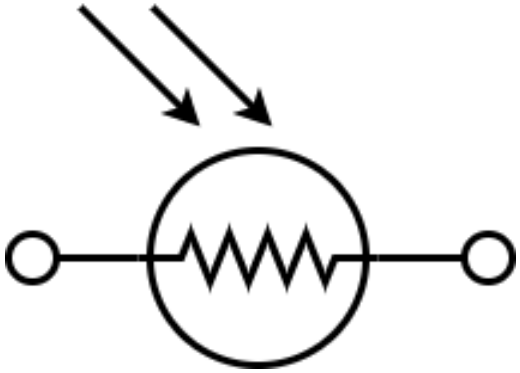

Figure 8. Photoresistor symbol (reproduced from [15]).

The equivalent circuit for an LDR could be considered to just be a variable resistor, where the incident light adjusts the resistance. [15.]

Compared to photodiodes and -transistors, photoresistors are cheaper and simpler to use to detect light. They do not have a p-n junction, but are made from semiconductor materials, and they rely on the photoconductive response. [15.]

Working principle of a photoresistor is that when light hits the material with enough energy to free an electron, the otherwise poorly conducting substrate gains mobile charge carriers through the photoelectric effect, and the resistance of the material falls substantially. [6,314-318.]

Disadvantage of photoresistors is their slow response time. The conductivity rises within tens of milliseconds, but it can take up to a second to reach the high resistivity state after the light is no longer applied. This resistance recovery time reduces the photoresistor applications, they are used for instance in streetlamps. [15.]

## 3 Measurement Setup

The measurement setup in its entirety is illustrated in Figure 9. It includes a light source, a monochromator, the testboards with the photodetector as the device to be tested (DUT), and other auxiliary equipment.

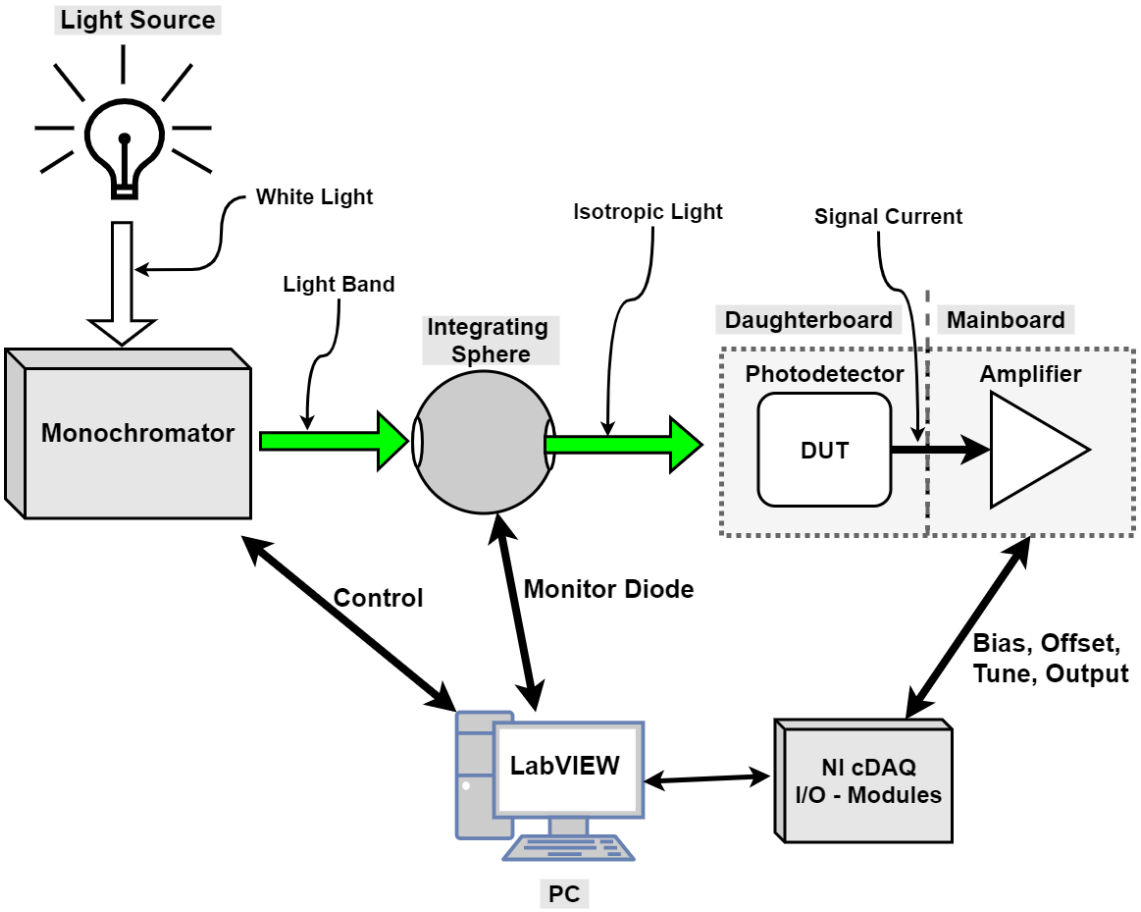


Figure 9. Measurement setup.

The measurement system in Figure 9 is controlled with a LabVIEW-program. The amplified signal is polled by NI cDAQ -modules for light bands of varying wavelengths provided by the monochromator and referenced by the monitor diode. The main part of the assembled measurement setup is shown in Figure 10.

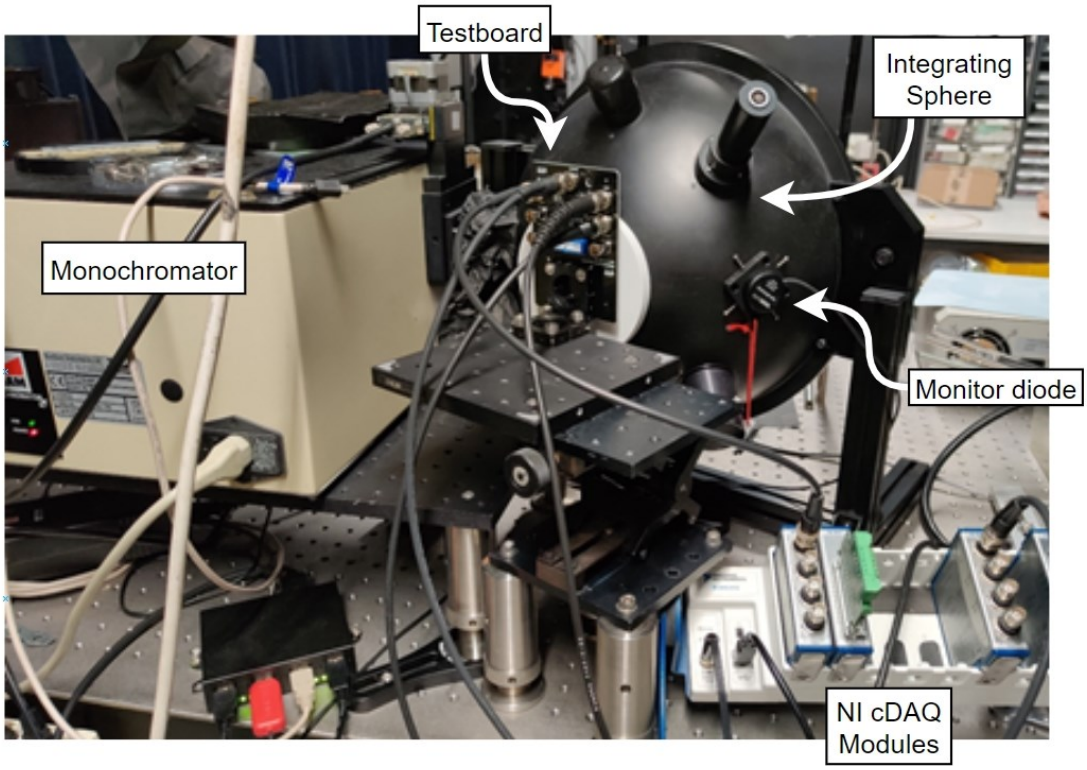


Figure 10. Assembled measurement setup.

Figure 10 illustrates how the equipment is assembled together in practice. Since any additional stray light might affect the measurement results, the light from the source is emitted only to the monochromator, and the whole measurement setup is in a darkened room. Most of the equipment, as well as the testboards, are colored black to absorb excessive light.

## 3.1 Light Source

The light is provided by an Osram 64657 HLX -halogen lamp. It has a power rating of 250 W and a nominal luminous flux of 9000 lumen. The lamp is bright and gives a wide spectrum of visible wavelengths, so it can be used as a light source for many optical measurements. However, a large portion of the lamp's power converts to heat and infrared radiation. The actual optical power for each wavelength in the spectrum is unspecified, but it can be taken into account by monitoring the light with a calibrated monitor diode. The spectrum of the light should have sufficient optical power at the wavelengths

of interest. The unfiltered white light from the lamp is fed into the monochromator device. [16.]

## 3.2 Monochromator

Monochromator is a device that provides a specified spectral band of light. They consist of a prism or a diffraction grating, mobile slits, and lenses and mirrors for directing and focusing the light beam. The diffraction grating is chosen so that the refractive index is appropriate for the wavelengths of the light source. The grating disperses the white light to a spectrum of its wavelengths as pictured in Figure 11. A prism can also be used for this purpose.

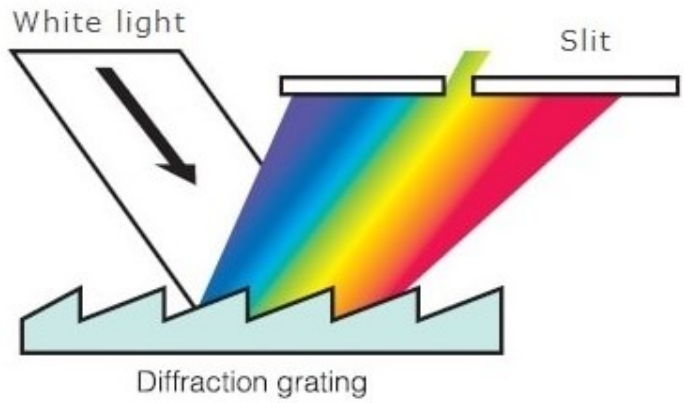


Figure 11. Working principle of monochromators. [17]

The motorized slits allow the specified band of light to pass through to the test subject, as shown in Figure 11. The resolution of the measurement is better with narrower bandwidths, but in turn the optical power of the incident light is smaller. The bandwidth should be large enough to get a measurable response from the detector. A bandwidth of 5 nm has been commonly used with this device. The wavelength is swept across the optical range with steps of 2 nm, which gives a more defined spectral response curve. [18.]


Figure 12. Bentham TMc300 Monochromator. [18]

The monochromator used in this measurement setup is a Bentham TMc300 Monochromator, as shown in Figure 12. It has a wide optical range of 200 nm to 50 um. The diffraction grating installed to the monochromator is rated for wavelengths of 400 nm to 4500 nm. A LabVIEW library is used for interfacing with the device. [18.]

The optical power of the monochromator's output is unknown, and it is affected by changes like flickering of the light source. A calibrated photodetector can be placed in the same location as the device under test (DUT), to have a reference level, so that measurement results could be scaled accordingly. Another method of acquiring the magnitude of the optical power, is to use an integrating sphere with a monitor diode, which is applied with this setup.

## 3.3 Integrating Sphere

An integrated sphere is a piece of equipment, that diffuses the light beam. This reduces errors from the angle dependency of the DUT. The light beam input to the integrated sphere is reflected around the highly reflective inside surface of the sphere, which makes the light isotropic, so the optical power does not depend on the direction of light. However, a small amount of optical power is lost in diffusion. Since the lighting conditions are constant inside the sphere, the optical power is measured in this stage by a monitor diode. The integrating sphere used in this setup is a 12" Gamma Scientific GS-IS300,

and the monitor diode with it is Thorlabs PM16-120, which connects to the PC with an USB cable. The working principle of the integrating sphere can be seen in Figure 13. [19.]

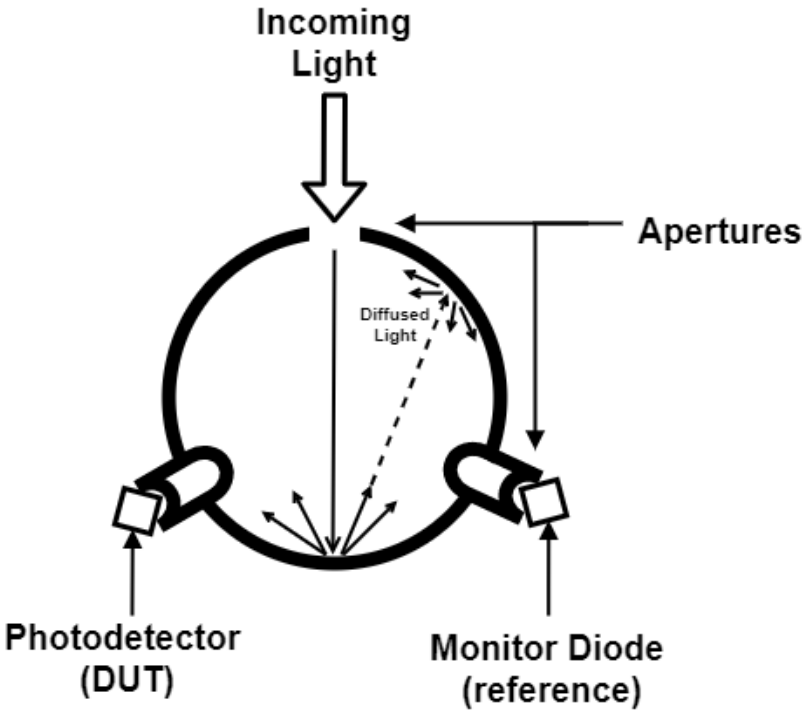


Figure 13. Principle of an integrating sphere

The DUT should be sealed against the output of the sphere, so that light does not needlessly escape. In case that the DUT is not at the same exact distance from the surface of the sphere as the monitor diode, another detector placed at the same location as the DUT can be used to calibrate the optical power levels.

## 3.4 Testboards

The daughterboard with the photodetector, is fixed against the integrating sphere. It is connected to the mainboard, which amplifies the signal. These testboards and amplifiers are described in more detail in the next two chapters.

The amplified signal from the mainboard is passed to a NI cDAQ input module. Another NI DAQ module is used to pass biasing voltage levels to the testboards. The mainboard is powered by a laboratory power supply, and it is connected to the cDAQ modules with coaxial cables.

## 3.5 LabVIEW and NI cDAQ Interface

The method of controlling the measurement system is a LabVIEW -program, so it is practical to use NI cDAQ I/O modules for data acquisition, as they are compatible with the software and have a sufficient accuracy. Additionally, the testboards are used with bias, offset and tune voltages. These voltage levels are passed through to the mainboard by an NI 9263 analog output module, and an NI 9215 is used for data acquirement. Both of these modules have the following features:

- 4 Channels (BNC Connectors)
- 100 kS/s/channel
- Voltage Range: ±10 V
- 16-Bit Resolution [20;21.]

This whole procedure is controlled with a LabVIEW-program on a PC. The LabVIEW VI contains many sections related to the measurement setup control, but as an example Figure 14 shows the data acquirement block diagram.

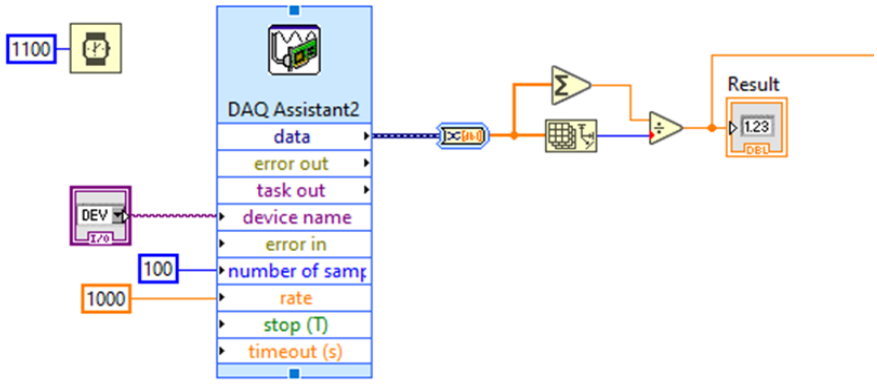


Figure 14. Block diagram of the measurement function in the VI.

As Figure 14 shows, one hundred samples are taken of the given wavelength step and averaged. The result is passed to the next case structure of the VI, which saves the result to a text file, and moves on to the next measurement step. The input voltages for are fed to the testboards similarly with a DAQ Assistant -block.

## 3.6 Mechanics

Devices to be measured are typically fixed at the ends of four rods with screws. These four rods are a part of a cage system, as shown in Figure 15, which enable the DUT to be moved along only one axis, if needed.

Figure 15. Mounting system, rods with cage plates. [22]

The mounting system in Figure 15 is holding cage plates, that keep the rods in place. There is a variety of modular mechanical parts, so they can be combined to firmly fix the DUT to any desired location. In this setup the testboards are screwed to an adjustable assembly platform with a right-angle cage plate.

The diameter of the mounting rods is 6mm, and they have 2.5 mm screw threads at the ends [22]. The testboards have drill holes for these apertures with the same 3 mm intervals as the cage plates for an easy installation.

# 4 Photodetector Amplifiers

The signal current through a typical photodiode is in the order of tens or hundreds of microamperes. To conduct measurements and research, it is practical to convert this signal to a common 0 V to 5 V logic level, so that it is within the full range of most ADCs. Measurement data can then be more easily processed and analyzed digitally.

## 4.1 Operational Amplifier Properties

Ideally an amplifier has no offset, is fully linear, and its operation is not affected by the signal source or the load, or vice versa. Transistors are the basic building blocks for an amplifier, they can amplify by themselves, but from a design point of view, ready-made operational amplifiers (op amps) are more applicable. Op amps are closer to an ideal amplifier, they contain tens of integrated transistors to provide differential inputs and a more linear output. [23,21-29; 23,43-49.]

The unideal properties of a real op amp should be examined when designing a circuit. When accuracy is needed, important parameters to consider in all applications involve noise. Power supply rejection ratio (PSRR) signifies how well the op amp rejects noise from the power supply, which can also be combated by filtering the supply. Similarly, common mode rejection ratio (CMRR) should be of sufficiently high value, it measures how well the op amp rejects the common mode voltage, which appears at both inputs. Regarding noise minimization the inherent voltage and current noise levels of the op amp should also be minimal. [23,81-84.]

To have a good measurement range, the op amp should be rail-to-rail for both input and output. The signal source is often connected to the same supply voltage as the amplifier, which often requires the use of full dynamic range of the op amp. Output should swing close to the supply voltage to achieve a good input to output response. However, even rail-to-rail output amplifiers still fall short from reaching the supply voltage level with some millivolts. Op amps with rail-to-rail input are much less common, and this problem may also be compensated by applying a small common mode voltage to the inputs instead of ground. Inputs of the op amp additionally have a small offset voltage which can provide a significant error if the amplified signal is small. This input offset can drive the output to either rail, especially with large gain. Op amp inputs also do not have an ideal infinite impedance, but there is a small leakage current going through the inputs, which can create an offset voltage at the output. Typically, there is some capacitance between the inputs, which is especially noteworthy in high frequency applications, as it affects the stability of the op amp. This can be compensated by adding a feedback capacitor, which counteracts the pole in the transfer function of the amplifier circuit. [24;25.]

The op amp should be able to provide enough gain without saturation for the application. If a large gain is required, multiple op amps can be cascaded together to prevent saturation. For all op amps the bandwidth is limited, it should be chosen to be adequate, as it cannot be extended by external components. In dynamic conditions where there are temperature changes, the temperature drift should be taken into account. [26,29-45.]

## 4.2 Current Amplification Circuits

Amplification of a small current can be done cheaply with an op amp circuit, which often belongs in two categories: Transimpedance amplifiers (TIA), or current shunt amplifiers. Both of these amplifiers give an output voltage that is directly proportional to the current through the signal source, in an ideal case.

### 4.2.1 Transimpedance Amplifiers

In this project the photodetector is thought of as a photodiode, and transimpedance amplifiers are usually associated with photodiodes. The photodiode can be used in different

modes by biasing it or connecting it between the inputs of the op amp. Figure 16 shows these two different modes. [27.]

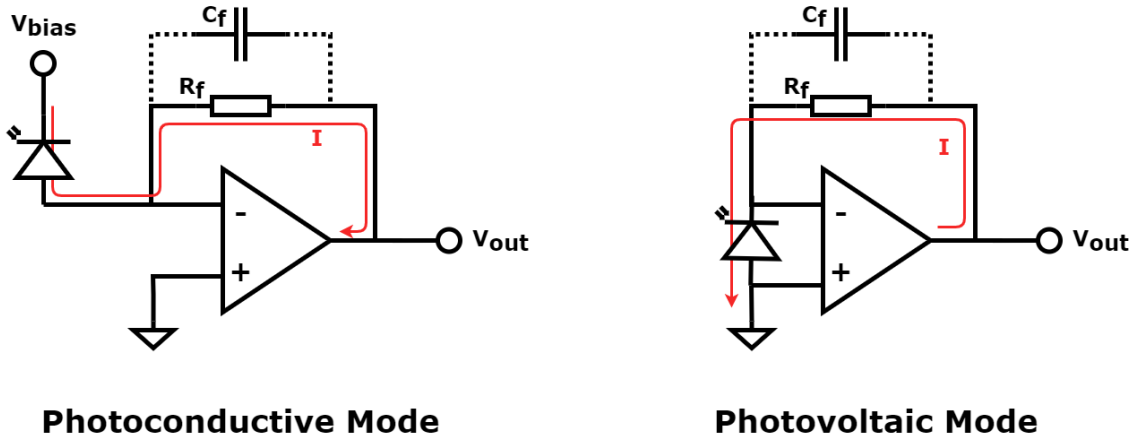


Figure 16. Photodiode configurations in TIAs.

The photoconductive mode in Figure 16 is the most common mode of using a photodiode. A reverse bias applies the external electric field to the junction of the diode, which drives the charge carriers when they are separated in the electron-hole photogeneration. This provides the largest and the fastest response to incident light. If the photodiode is forward biased instead, the light response is significantly weaker, the component acts in the same way as if it were an LED with very low efficiency.

If the photodiode has no bias across it, it works in a photovoltaic mode as shown in Figure 16. This is similar to how a solar cell works. The photogeneration of separated charges is detected as a small voltage across the photodiode. This mode minimizes the dark current along with noise. However, the capacitance of the junction is increased by the input capacitance of the op amp, which results to slower response times.

To calculate the output voltage of a transimpedance amplifier, the Kirchhoff's voltage law can be used to provide the equation 4.

$$V_{out} = I * R_f \tag{4}$$

Equation 4 shows that the output voltage $V_{out}$ is simply the product between the signal current I, and the feedback resistor $R_f$.

Due to the combined capacitance of the photodiode and the input of the op amp, a compensation capacitor $C_f$ is optionally added in parallel to the feedback resistor to stabilize the amplifier. This implements a low pass filter with a cutoff frequency $f_c$ as defined in equation 5. [27.]

$$f_c = \frac{1}{2\pi R_f C_f} \quad (5)$$

Where the $C_f$ is the feedback capacitor. Likewise, if a serial capacitor is placed at the signal input, it implements a high pass filter. These options are often used depending on the application to reduce noise and can also be combined to form a band pass filter.

### 4.2.2 Current shunt amplifiers

Current shunt amplifiers are used more generally to measure currents using op amps. This method is used more often with larger currents. The idea of a current shunt amplifier is that the op amp amplifies the voltage drop over a sense resistor, through which the same current flows as through the signal source. The placement of the sense resistor, load and the feedback can change depending on the application. The Figure 17 shows an example of a low side, and a high side current sensing circuits.

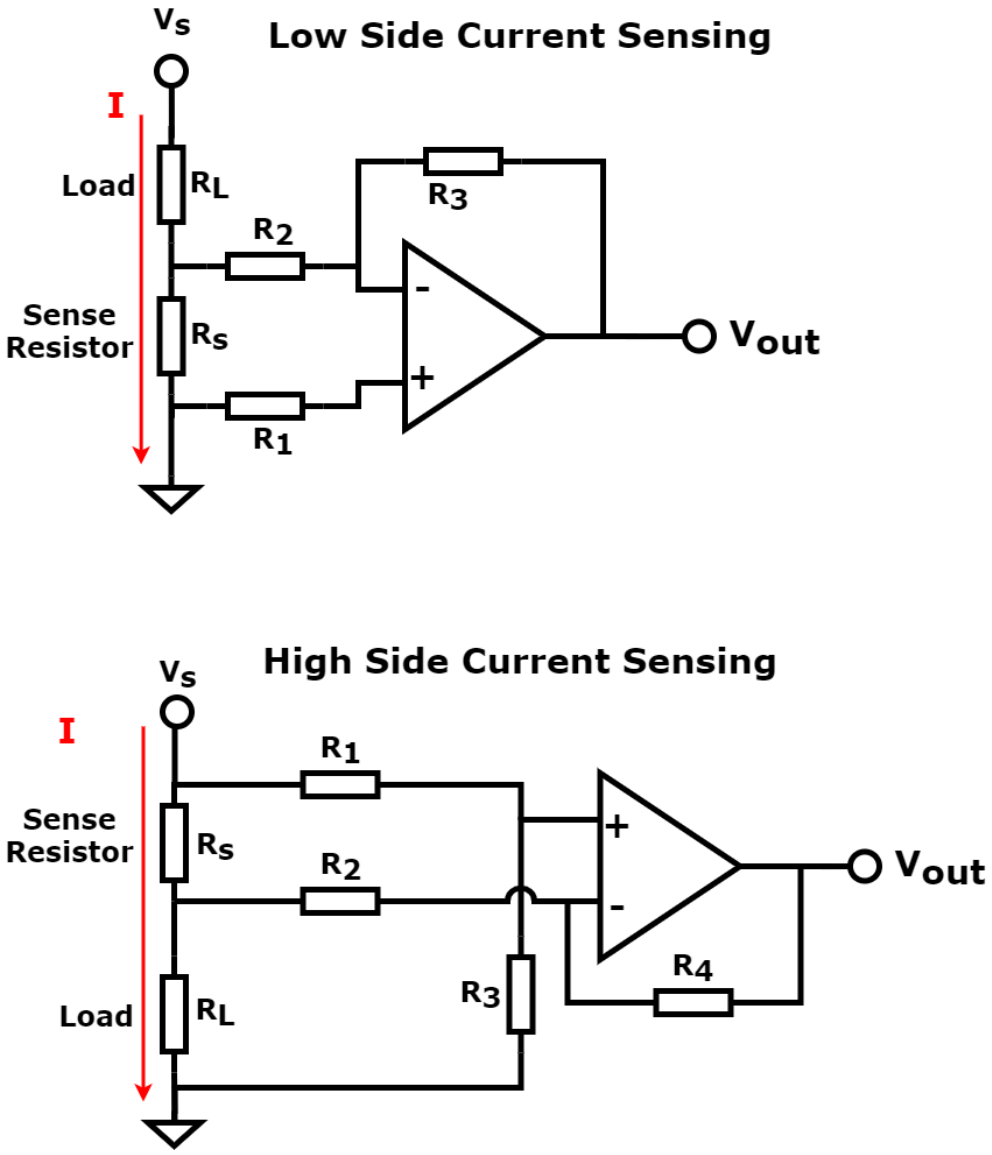


Figure 17. Current shunt amplifier circuits.

Both circuits in Figure 17 use the op amp in a configuration known as a differential amplifier. In this configuration the resistors $R_1$ and $R_2$, and $R_3$ and $R_4$ are usually matched to be the same, which gives the output voltage in equation 6.

$$V_{out} = \left(\frac{R_3}{R_1}\right) * R_s * I \quad (6)$$

Where $V_{out}$ is the output voltage, $R_s$ is the sense resistor, and I is the current through it, also for the resistors $R_1$ equals to $R_2$, and $R_3$ equals $R_4$. The low side example has the

sense resistor between the ground and the load, so the load is referenced against the supply voltage. This means that leakage from the load to ground does not go through the sense resistor. The high side current measurement circuit has the sense resistor against the supply voltage, hence all of the current through the load will flow through the sense resistor as well. In this case the inputs of the op amp have a high common mode voltage, requiring a high CMRR. These circuits can be found integrated in devices called funnel amplifiers, which contain a selection of precisely matched resistors for accurate measurements. It is important to accurately know the values of the resistors since they all have a direct effect to the output. [28.]

## 4.3 Implemented Amplifier Circuit Designs

Two different amplifier designs were carried out, a transimpedance amplifier and a current-to-voltage converter. They were built so that the user could select between them and choose the amplifier which gives better results. The detailed schematics of the designs are attached as appendices 1 and 3, Mainboard schematic, and Daughterboard schematic, respectively.

**Transimpedance Amplifier's** functional circuit diagram can be seen in Figure 18.

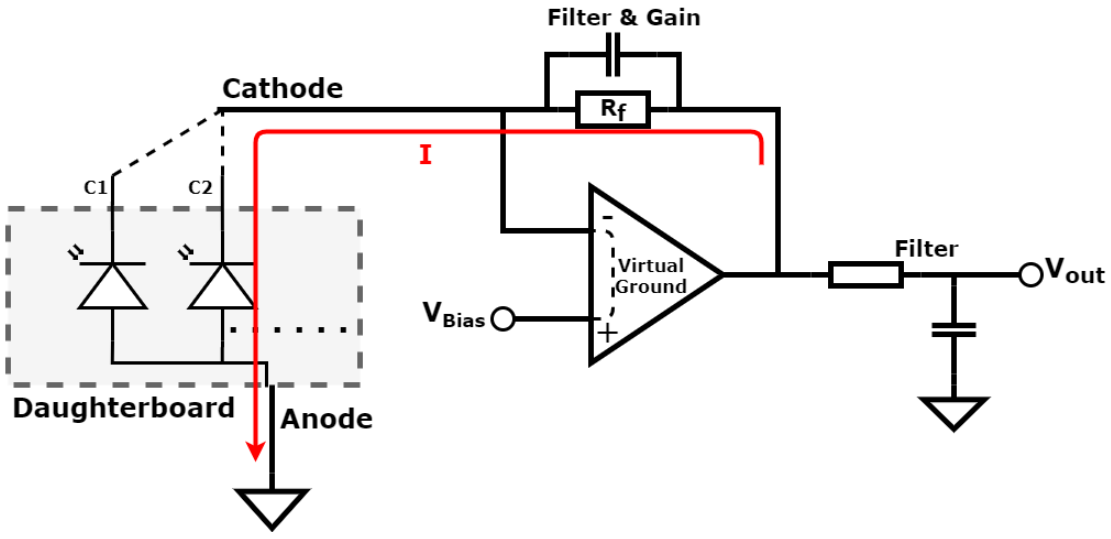


Figure 18. Transimpedance amplifier implementation.

As shown in Figure 18, the daughterboard holds multiple photodetectors, which can be selected individually with a switch. In this design the anode of the photodetector is connected to ground, while the cathode is biased through the virtual ground of the op amp. The current through the op amp's inputs is negligible compared to signal current, so the current passing through the feedback resistor is the same as the signal. The output feeds the inverting input of the op amp to keep it in the same potential as the non-inverting input. Therefore, the voltage across the photodetector is the same as the bias voltage applied. The photodetector can also be measured with zero bias by physically grounding the bias connector.

The disadvantage of this amplifier is that the output voltage is limited by the bias voltage since it applies a common mode voltage to the op amp. The signal current through the detector can be measured from zero to its maximum by decreasing the feedback resistance, but still the output swing is from the bias voltage to near supply voltage level. If the bias node is grounded and the anode is connected to a below ground level voltage, measurements in reverse bias mode can be achieved without a common mode voltage limiting the output.

A parallel capacitor in the feedback is used to compensate the combined capacitance from the photodiode junction and the op amp's input. The unwanted input capacitance creates a lowpass filter at the input of the op amp making the gain potentially unstable. This is not likely to happen with low frequencies, but the feedback capacitor is still added to reduce noise, additionally another low pass filter is placed at the output to further attenuate high frequency signals.

The equation for the output voltage of the amplifier $V_{out}$ is given in equation 4.

$$V_{out} = I * R_f + V_{Bias} \tag{4}$$

Where I is the signal current, $R_f$ is the feedback resistor, and $V_{bias}$ is the reverse bias voltage.

**A Current-to-Voltage Converter** was additionally designed to nullify the effect of the output range limitation with increasing bias voltages. The photodetector is reverse biased

by a voltage follower, with a current limiting resistor added to its output. The diagram for this design is illustrated in Figure 19.

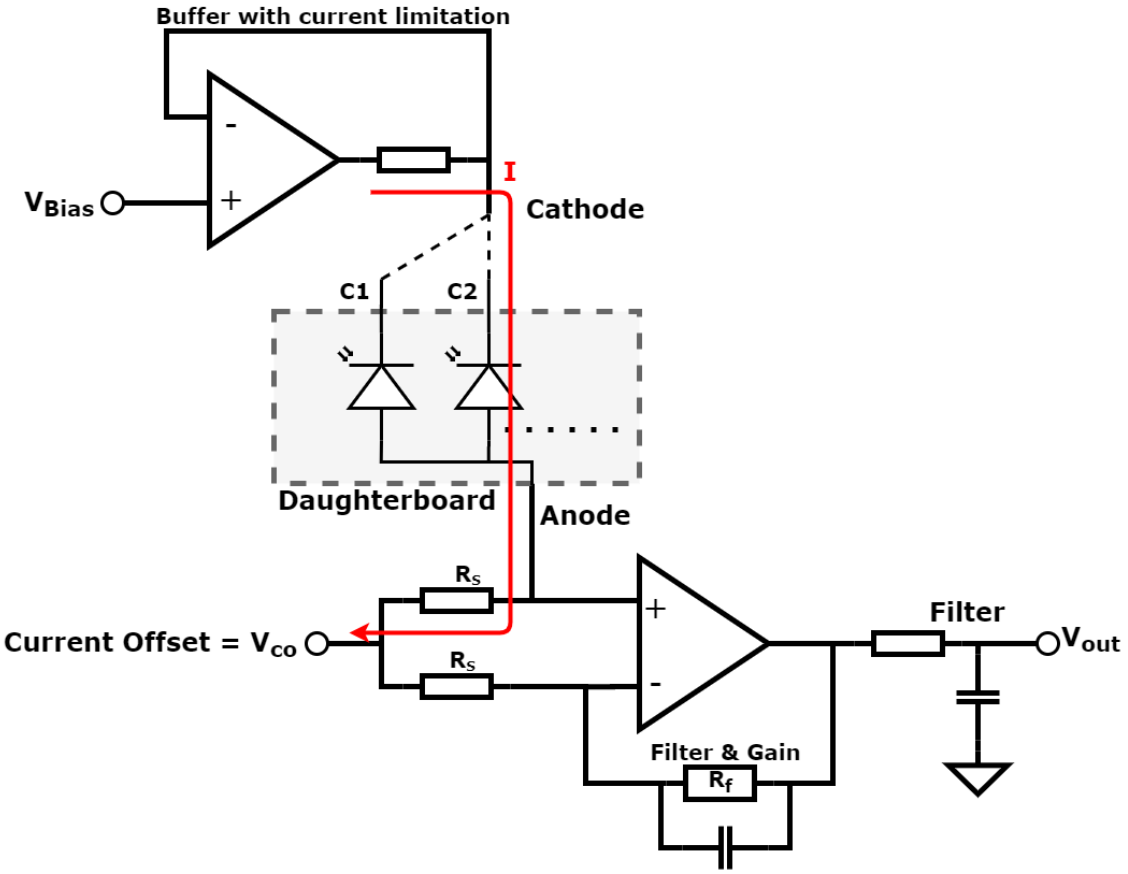


Figure 19. I-V Converter implementation.

The amplifier circuit is similar to a low side current shunt circuit without a complete differential configuration. The voltage drop across the sense resistor $R_s$, shown in Figure 19, is directly proportional to the current through it, which equals to the signal current.

Here, the inputs of the op amp are connected to a low voltage called current offset, instead of ground. This is done to elevate the signal off from the lower rail to the linear region of the amplifier, so that even small currents can be measured accurately. The current offset can also be applied to the anode in TIA circuit to get the same benefit. Both inputs are connected to the current offset through the same resistance, so it does not provide an asymmetry to the inputs, for this reason also the loop between the inputs

should be minimized, as well as the feedback loop. Gain, filtering and decoupling properties of this circuit follow the same approach as in the TIA's design.

The output voltage $V_{out}$ can be related to the signal current as in equation 5.

$$V_{out} = I * R_s * \frac{R_f}{R_s} + V_{co} = I * R_f + V_{co} \quad (5)$$

Where I is the signal current, $R_f$ is the feedback resistor, and $V_{co}$ is the current offset voltage. The amount of bias voltage does not affect the output as in the TIA design.

# 5 PCB Design

## 5.1 Overview

Two testboards were designed in PADS program, a daughterboard, where the photodetector is installed, and a mainboard, which contains the amplifiers and other required parts. The designed layout of the mainboard can be seen in appendix 2 and the layout of the daughterboard is shown in appendix 4. The overview of the testboards' design and its contents are shown in Figure 20.

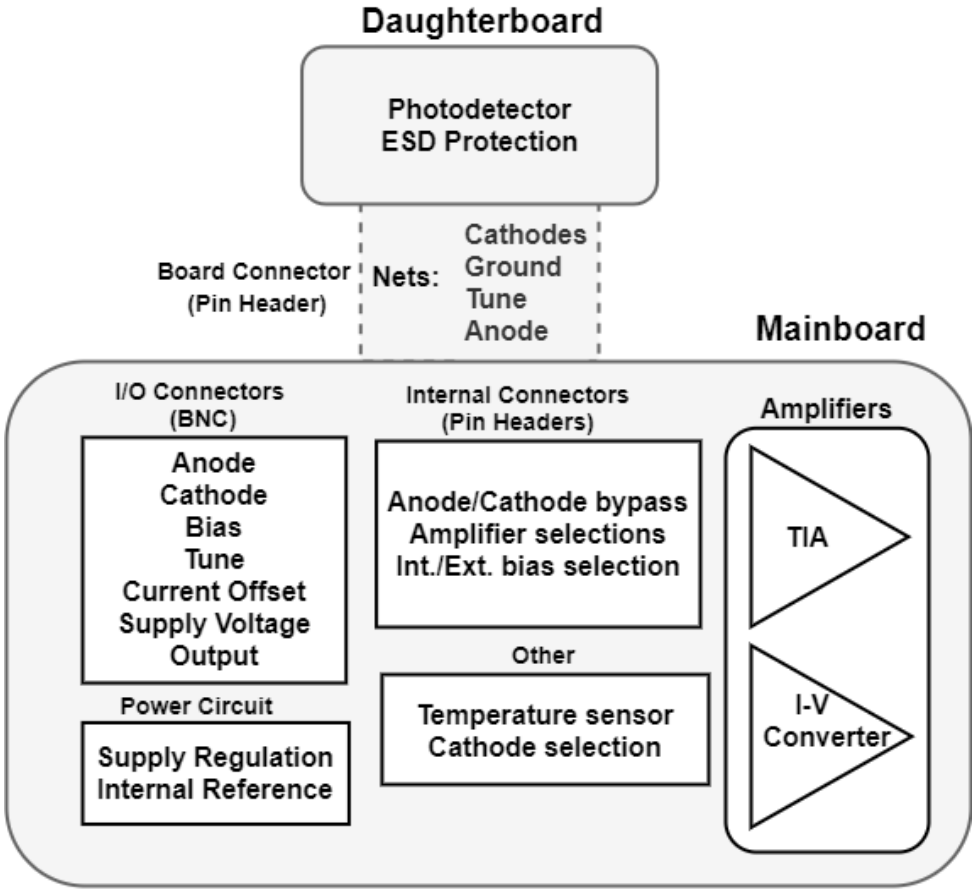


Figure 20. Contents of the testboards.

As shown in Figure 20 two different amplifiers were implemented on the mainboard, which could be switched or configured with using terminal blocks. The mainboard also housed the necessary power and biasing voltage circuits, and BNC connectors for interface. The daughterboard is connected to the mainboard through a 14-pin header, connecting the nets from the photodetector to the mainboard.

Measurements required that the photodetector could be firmly fixed to a defined distance away from the light source, so that the measurements could be replicated. This made requirements to the mechanical layout of the PCBs. Both sides of the testboards PCBs are shown in Figure 21.

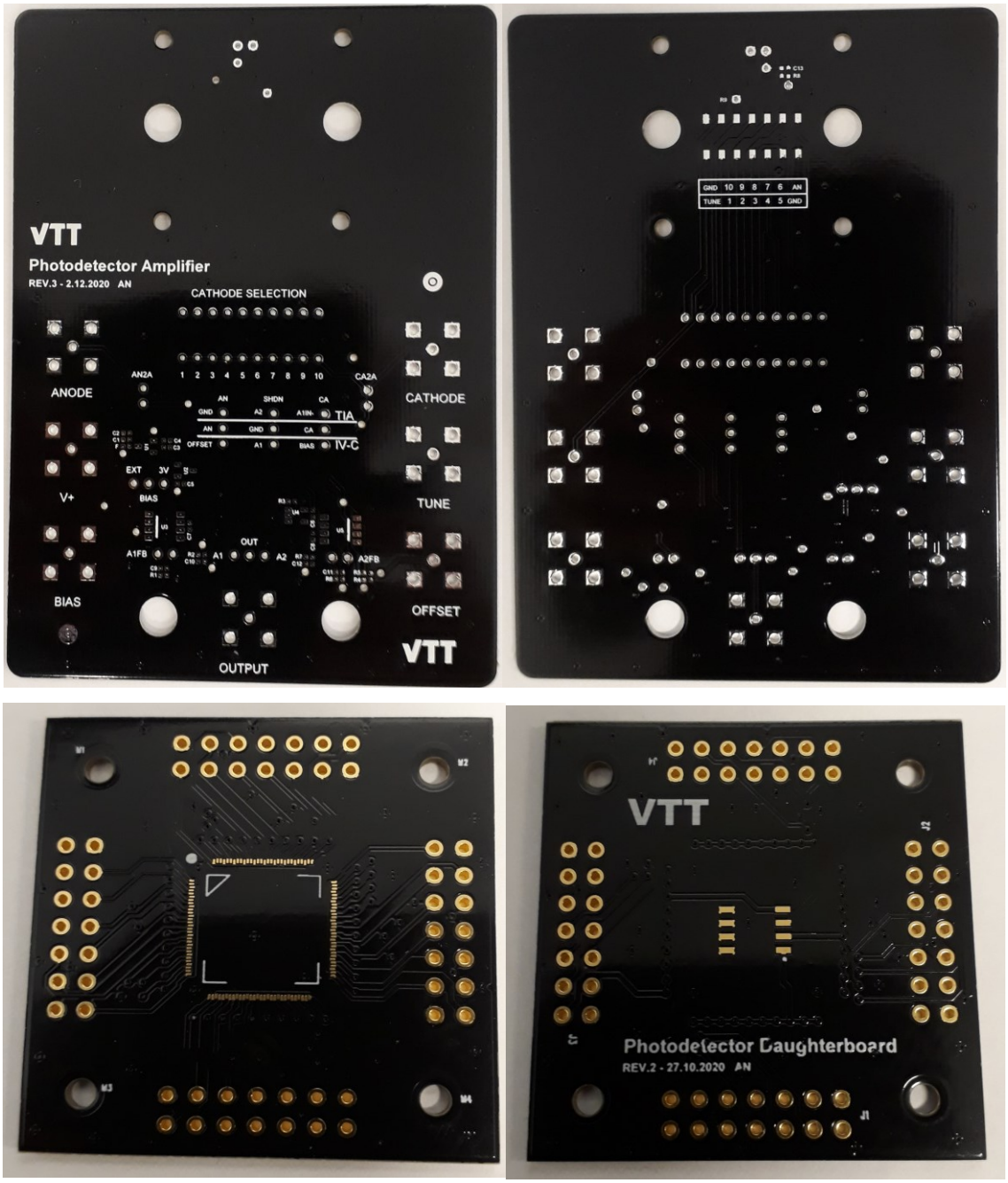


Figure 21. Top row (from left to right): Top, and bottom of the mainboard
Bottom row (from left to right): Top, and bottom of the daughterboard.

The ground layers of the testboards in Figure 21 were stitched together with vias to improve electromagnetic interference rejection properties of the boards. Vias were also used as test points with some important nets, like supply and bias voltages.

**Amplifiers** were implemented on the mainboard as described in the previous chapter. The op amp was required to have a low noise level, rail-to-rail output, and a 5 V operation voltage level, low input current and capacitance were also preferred. Three op amp chips were simulated for the TIA circuit in LTspice, LMH6611, LTC6228, and LTC6268. The LTC6268 op amp produced the best response by having the lowest output offset and the highest saturation point, so it was chosen to be used. [29.]

According to datasheets it is recommended to add a 100 nF decoupling capacitors between the power and ground pins, as close as possible to the integrated circuits (ICs). The feedback loop is also to be kept as small as possible, to reduce magnetic coupling. [29; 30; 31; 32.]

The signal current was initially estimated to be in the range of 0 to 500 uA, so the default gain resistors of the amplifiers were rated to produce a gain of 10 000, to have a 0 to 5 V output. In this setup, the highest sampling frequency is only 1 kHz, so a 100 kHz cutoff frequency is used to filter out high frequency noise, which is also far from the Nyquist frequency, so filtering does not affect the result of the signal.

Additionally, decals for two-pin female headers were added in parallel to the feedbacks of the amplifiers, so that before the gain resistor is soldered on, a variety of resistors could easily be tested to determine the appropriate gain, as the actual current range of the DUT is unknown before testing.

The IC used in the voltage buffer for the I-V converter was chosen to be a TLV9051 op amp, which is cheap and commonly used for buffering. [30]

**Supply voltage** for the amplifiers is provided by an external power source through a voltage regulator circuit, in case that the power source is noisy. The power is fed through a ferrite bead and over decoupling capacitors to a MCP1702 voltage regulator, to provide a stable 5 V supply. The output of the voltage regulator is also fed to a MAX6103 voltage reference device, which outputs a stable 3 V reference voltage to be used as an internal bias voltage option. Decoupling capacitors are placed close to the input and output of the MAX6103 chip. In the layout these components are placed near the power supply connector. [31,32]

**Temperature sensor** circuit was added to the mainboard for future research purposes. It encompasses a voltage divider with a noise filter capacitor, and two pins near the edge of the PCB for readout. The temperature is sensed by a 100 kohm NTC thermistor B57164K0104J000, which is pulled up through a precision 100 kohm resistor to the 3 V reference voltage, which has a very low temperature drift. This makes the sensing circuit sufficiently accurate with only a few components. The NTC thermistor is disc packaged so it can be physically pushed against the daughterboard to have a better reading of the actual temperature of the detector. [33.]

**BNC connectors** were used as I/O connectors in the mainboard, since coaxial cables are resistant to electromagnetic interference, and they are commonly used by peripheral devices, including laboratory power supplies and NI DAQ modules. The anode and cathode connectors are not connected in normal use, but they can be used for example to directly access the anode and the cathode of the photodetector, if the amplification is bypassed. Other inputs are for current offset, bias, and tune voltages, and for the operating voltage supply. The tune voltage is reserved for example as additional bias, that could be used in future research. The output from the amplifiers is similarly accessed through a BNC connector.

**Pin headers** were utilized as the user interface for the mainboard. By either disconnecting or shorting two male pins together with a terminal block, the user could control the configuration of the circuit. All pin headers were chosen to have a gold finished surface, to provide a low impedance contact. The amplifier could be selected by connecting the anode, cathode and output nets to the appropriate amplifier inputs and outputs. The other amplifier can be turned off, by grounding its shutdown pin. The bias voltage can be chosen to be the internal 3 V reference, or it can be adjusted externally. The boards can also be used to just access the photodetector components' cathodes and common anode directly with BNC connectors, if the bypass pins are not connected to each other with a terminal block.

A **DIP switch** is used to select the individual photodetector component, which connects the corresponding daughterboard pin to the cathode net connected to the amplifiers. This can also be used to have a larger photoactive area, by connecting more than one component's cathode to the amplifier, since they are essentially connected in parallel.

**Mechanics** of the monochromator constrained the layout design of both boards. The sample was to be in the middle of 3x3 $mm^2$ square with a 2.8 mm drill holes in the corners, so it could be easily fitted to the mounting fixtures. Therefore, the daughterboard had 2.8 mm drill holes in a square pattern around the sample, for a similar installation as the cage plates had. However, the mainboard overlaps the daughterboard, when they are connected together, so 6 mm diameter drill holes were made on the mainboard, for the rods to go through. The drill holes of the mainboard and the daughterboard had to be concentric, and their centers had to be equidistant from the connector of the boards.

Four drill holes were also placed on the mainboard around the female pin header which connects the boards together, so that any photodetector component with legs could be easily installed for measurements. These two fixation methods are illustrated in Figure 22.

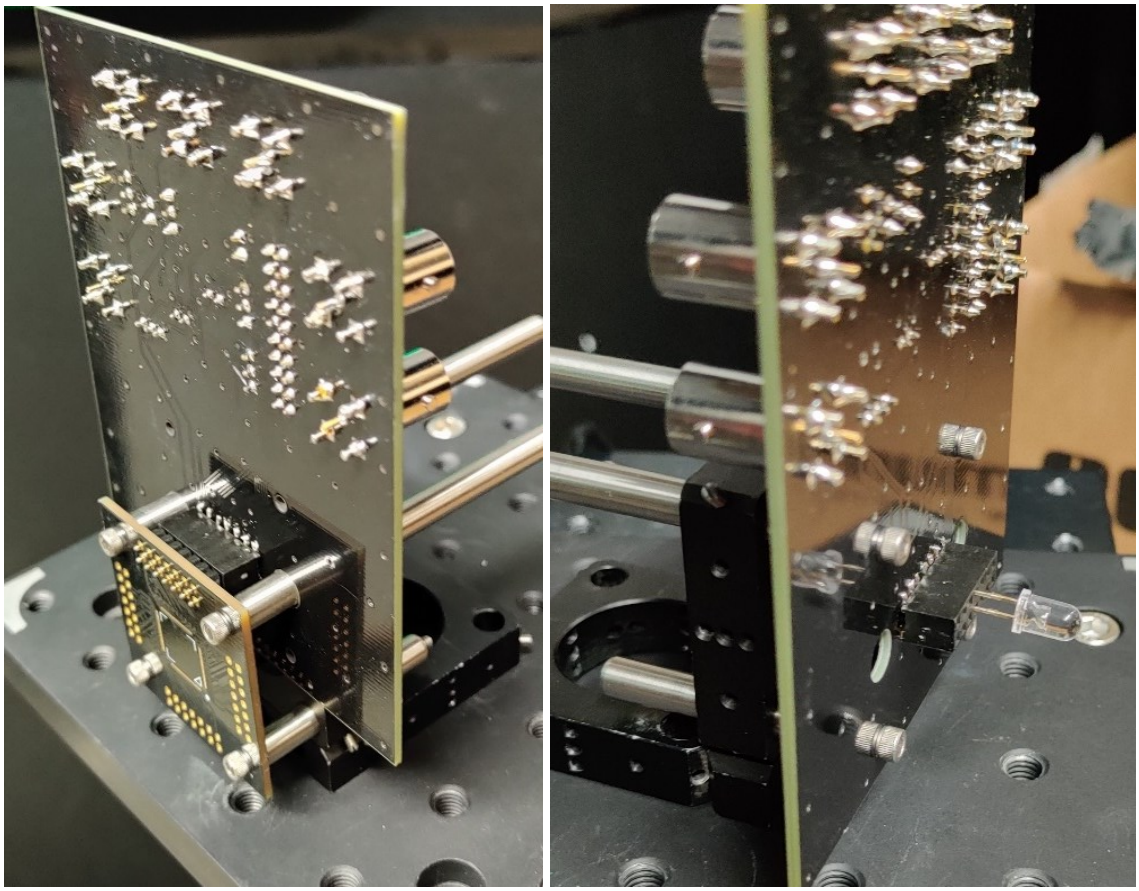

Figure 22. Two methods of using the testboards, with or without the daughterboard.

There are two additional drill holes on the bottom of the mainboard to add mechanical robustness, so that the device is not displaced when terminal blocks or connectors are removed or added.

## 5.2 Daughterboard

Multiple photodetector devices were processed on a silicon wafer and diced so that one chip contains 40 individual detectors. The chip is to be glued to the middle of the daughterboard PCB. It would then be bonded to the pads of the footprint made for the photodetector. The bonding pads on the PCB for the chip have gold finished surfaces, so that the bonding wires would be able to attach to the pads more reliably. Individual cathodes and other nets from it are connected to the 4 male pin headers on the sides of the board, so that the ten devices on each side of the chip can be accessed by the mainboard through the boards' connector.

The symmetry of the design was utilized so that every cathode could be accessed by the mainboard, by switching the orientation of the daughterboard. The pin order is the same for all 4 connectors on the daughterboard, so this avoids having 4 times as many pins on the mainboard.

There are no protective mechanisms against ESD on the photodetector chip, so a diode array SMDA15C-4-2TR is connected to the possibly vulnerable nets. [34]

## 5.3 Ordering and Assembly

The layouts of the testboards PCBs were exported into Gerber files, checked, and sent to Elecrow PCB for manufacturing. The narrow trace widths in the daughterboard layout, as well as the gold finishing on the pads, required the Premium service provided by Elecrow. The mainboard layout complied to the requirements of the regular Elecrow PCB manufacturing service. The color of the PCBs was selected as black, so the boards themselves have minimal effect on the measurement results. The components for the boards were ordered from Digi-Key Electronics. The assembled mainboard can be seen in Figure 23.


Figure 23. Assembled mainboard PCB.

Most of the components seen in Figure 23 were soldered with a reflow oven. Lastly, to make sure that the testboards fit mechanically together, they were screwed to the mounting fixtures before the board connectors were soldered in place. This way the testboards became perfectly aligned with each other.

The bonding wires of the photodetector chip on the daughterboard are exposed, since the chip cannot be fully enclosed, or it would not receive incident light. The bonding wires are very delicate, so a finger guard should be glued around the detector to prevent accidental damages. A simple finger guard can be made by sawing a ring from a PVC pipe, that is then glued around the chip. Additionally, a glass plate can be attached to the top, making the detector chip protected against moisture, as well as accidental touches, however the optical properties of the glass can affect the results.

# 6 Results and Discussion

The novel nanotechnology-based photodetector was still in production phase, so the performances of the designed amplifiers were verified with circuit simulations and measuring the output voltages for different amounts of current. The functionality of the measurement setup was also verified by characterizing two ready-made phototransistors and comparing the results to the values in datasheets.

## 6.1 Amplifier Performance

The amplifier circuits were simulated with LTspice Circuit Simulation Software, by implementing the equivalent circuit of a photodiode. Simulated circuits are shown in Figures 24, and 25. The biasing voltages were chosen to have values of 100 mV, 3 V, and 5 V, for both amplifiers. The current offset was grounded in all cases.

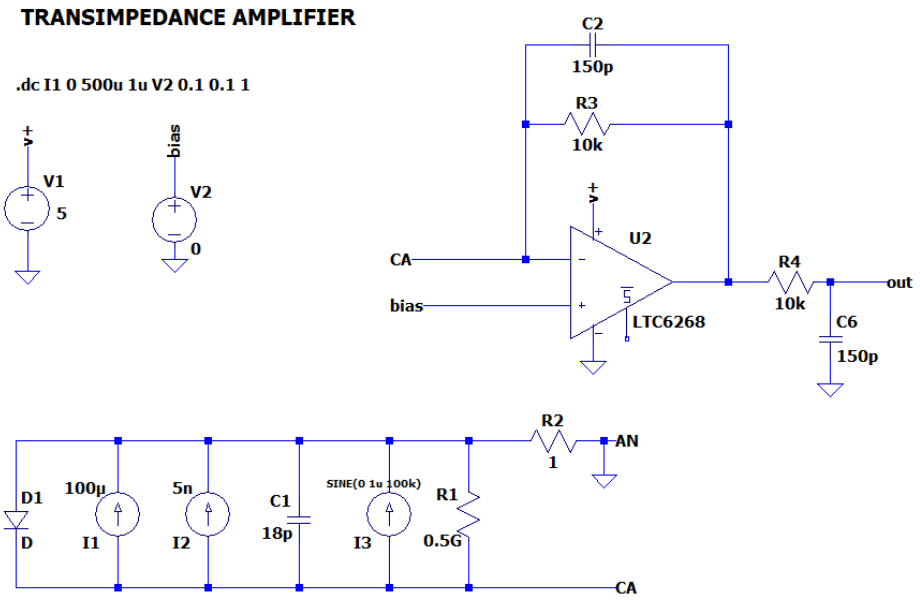


Figure 24. LTspice schematic of the TIA.

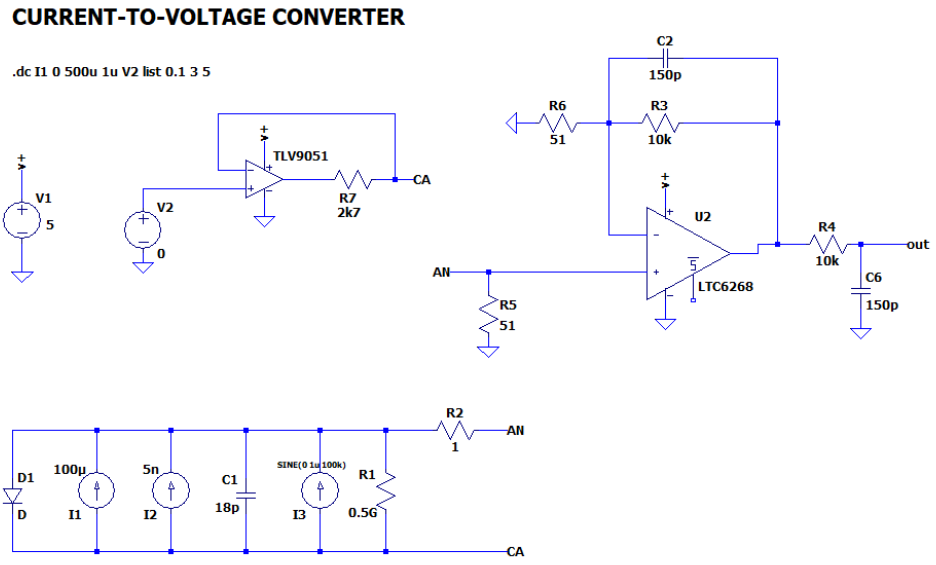


Figure 25. LTspice schematic of the I-V Converter.

The equivalent circuit components of the photodiode model in Figures 24 and 25 have exemplar values of a typical photodiode, Luna Optoelectronics PDB-C142. [35] The results of the simulations are compared to calculated output values for ideal amplifiers, which are extracted from equations 4 and 5 from the chapter 4.3. The comparisons for both amplifiers are shown in Figure 26.

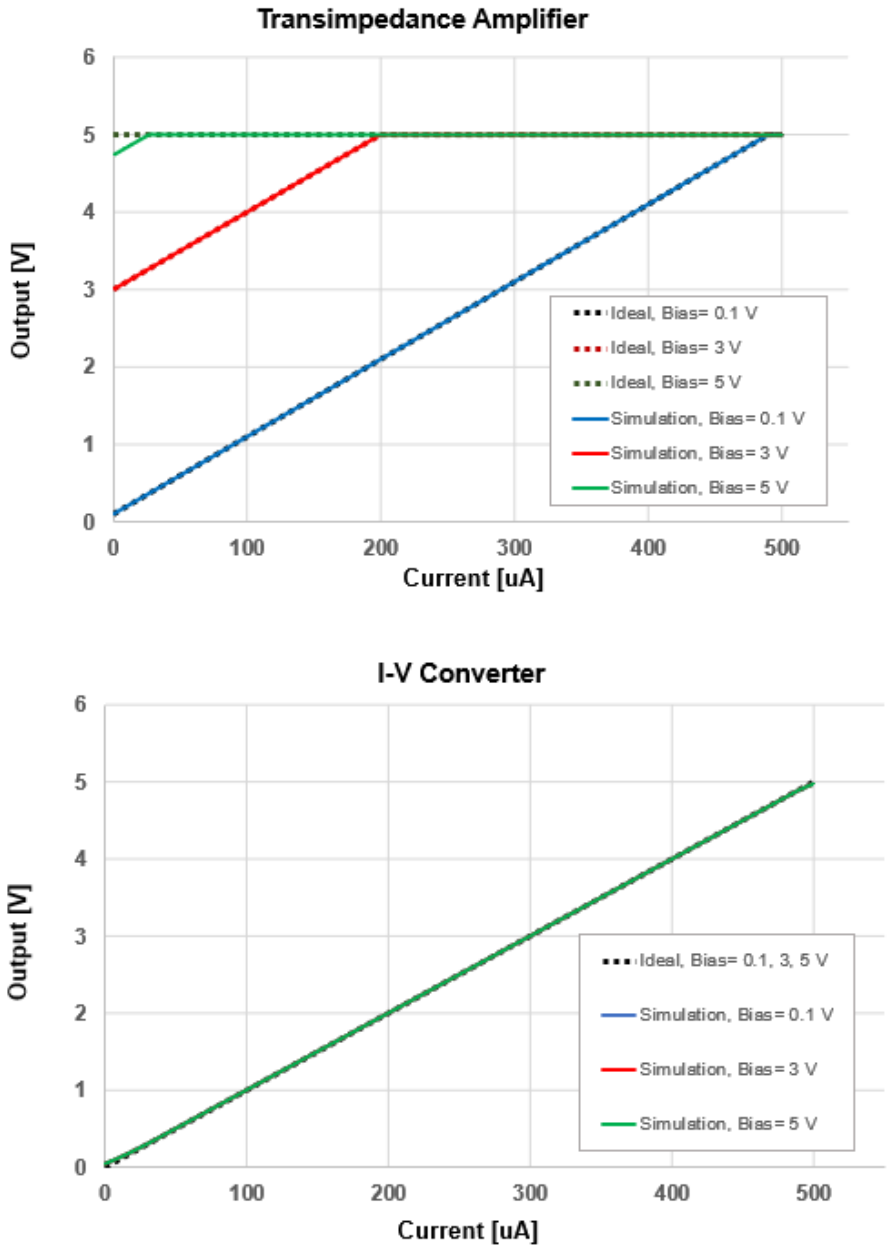


Figure 26. Circuit simulation results compared to ideal amplifiers.

Graphs in Figure 26 show that the output of the designed amplifiers is very similar to the ideal case. There is only a 0.2 mV output offset in the TIA simulation, apart from the case of 5 V bias, which already has a poor measurement range of the input. The I-V converter has a 47 mV offset at the output, so the current offset voltage of, for example 100 mV, should be used with it when measuring very small currents. The amount of bias seems to have no noticeable effect on the output of the I-V converter. The linearity of the output is very good in all simulated cases.

The performance of both implemented amplifiers was estimated by measuring the output voltage in respect to the signal current. The signal current was achieved by connecting various resistors across the anode and cathode nets of the circuits, in place of the detector. The measured output voltages of the amplifiers are compared to the simulated results in Figure 27.

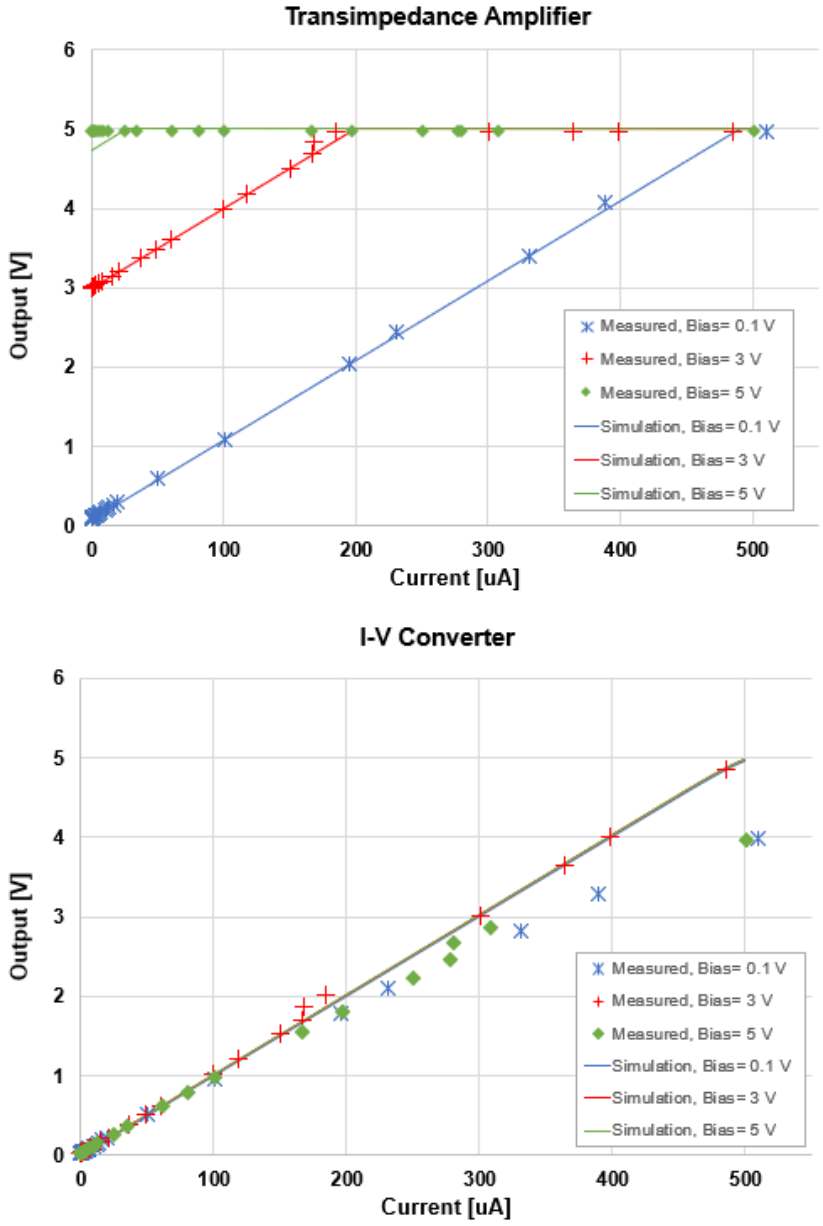


Figure 27. Measured output voltages compared to simulated results.

From Figure 27 it can be seen that the transimpedance amplifier follows the simulated results moderately well. There is a small amount of variation in linearity, and a larger discrepancy in the upper end of the measurement range. However, the graph shows that the transimpedance amplifier can be used to provide accurate readings of signal currents across most of the measurement range, especially with a low bias voltage.

The measured output of the I-V converter shows that the gain of the amplifier depends on the amount of bias voltage, the case of 3 V bias follows the simulated results, but with 0.1 V and 5 V biases the gain drops. This is likely because of the voltage follower unable to provide increasing amounts of current with a voltage level near its supply rails. There is also a bump in the midrange of the output with 3 V and 5 V biases. Otherwise, the response with a 3 V bias is quite accurate, and the output offset is 30 mV, which is less than in simulations.

The measurements show that the most accurate result should be provided by the TIA with a 3 V bias. This setting will be used to verify the performance of the measurement setup.

## 6.2 Comparative Photodetector Characterization

The performance of the measurement setup, including the mainboard, was evaluated with two ready-made phototransistors: Würth Elektronik 1540052NA3090, and Vishay BPW85A. The reference for the optical power density spectrum inside the integrating sphere was measured by the monitor diode PM16-120, the result is shown in Figure 28.

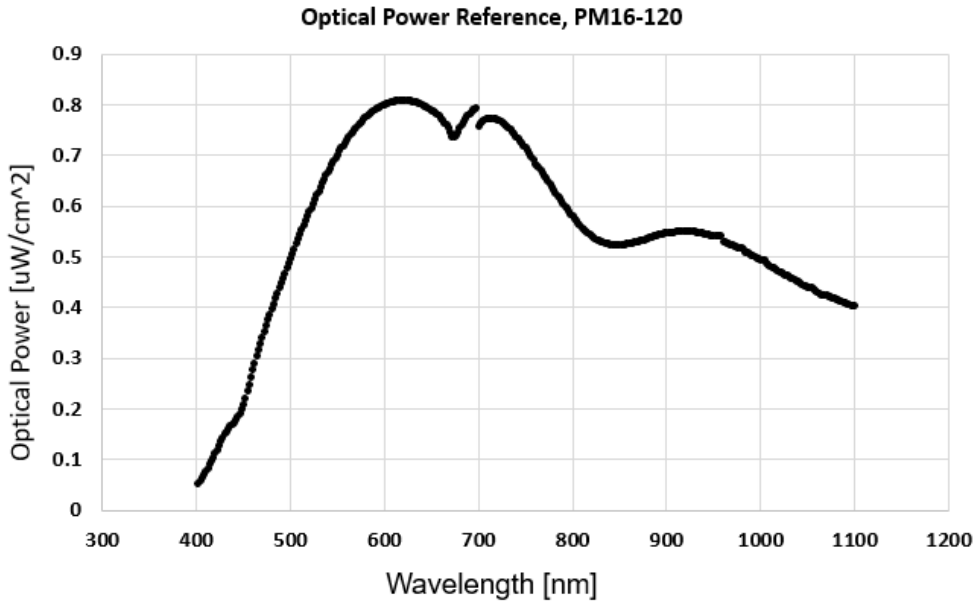


Figure 28. Optical power density inside the integrating sphere.

As seen from Figure 28, the optical power is only between about 50 to 800 nW/cm$^2$. This power is very low for the measurements to be done with a photodiode with the default gain of the amplifiers, but phototransistors have internal gain, so they produce a more detectable signal. The feedback components of the amplifier can be changed to increase the gain for future tests.

The results of the output voltages from the phototransistors can be seen in Figure 29.

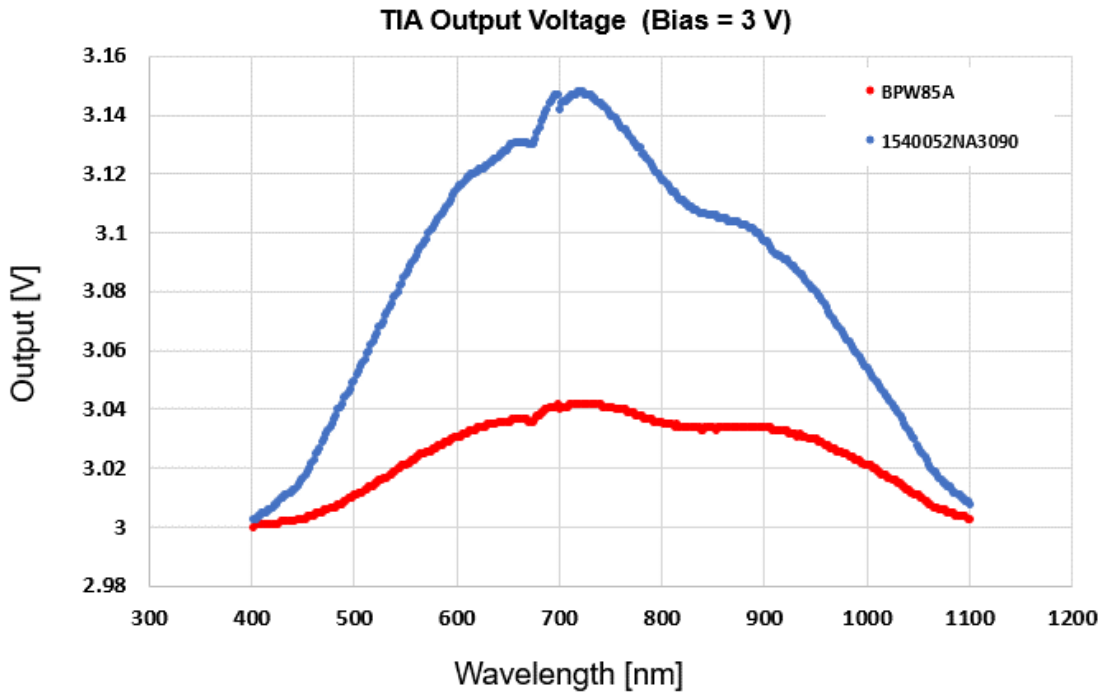


Figure 29. Measured output for the phototransistors.

The voltage change of the output is only about 150 mV for 1540052NA3090 and 40 mV for BPW85A. This is due to the amplification being rated for a much higher photocurrent, which would correspond to the optical power of 1 mW/cm$^2$, as given as the test condition in the datasheets. [36; 37] However there is enough resolution to interpret the results.

These output values are converted to signal current values using equation 4, and then it is referred to the optical power spectrum with equation 2, to get the spectral responsivity of the components, shown in Figure 30.

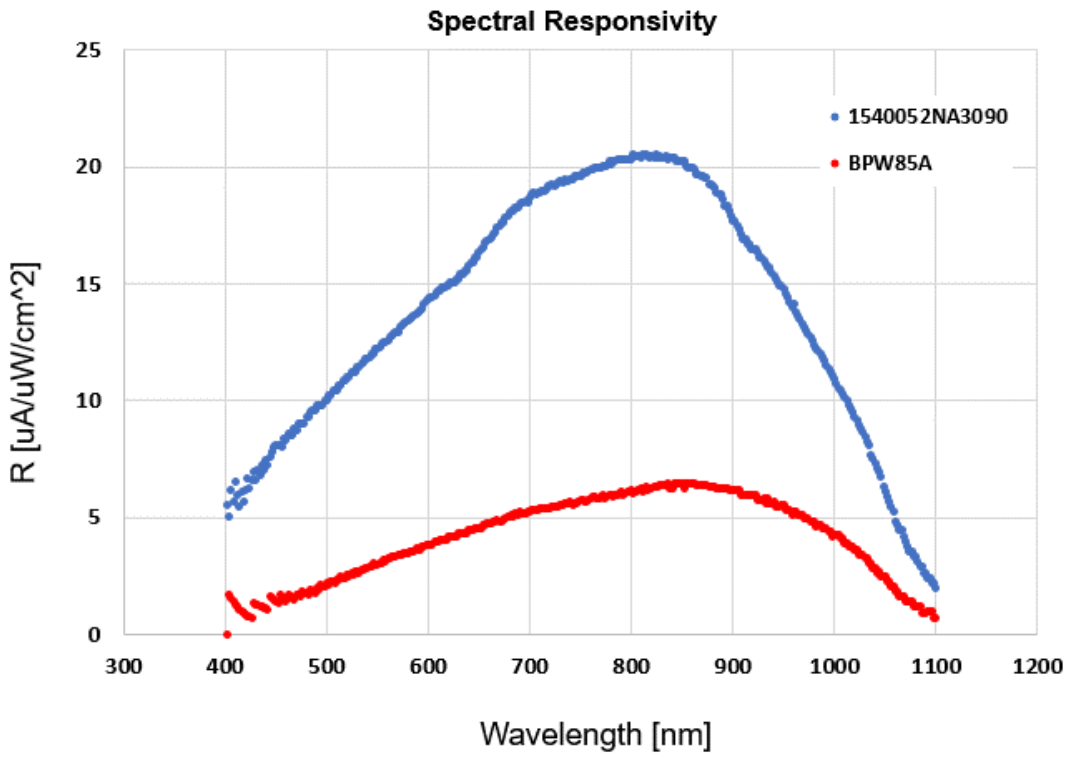


Figure 30. Measured spectral responsivity of the phototransistors.

The values for spectral responsivity in the components' datasheets are rated for 50 µW/cm$^2$ at the lowest, so proper conclusions cannot be drawn. However, to compare the relative spectral sensitivity of the components to figures in datasheets, the results in the Figure 30 are normalized to values between 0 and 1, so they can be compared to the graphs in the datasheets. These waveforms are compared in Figures 31 and 32.

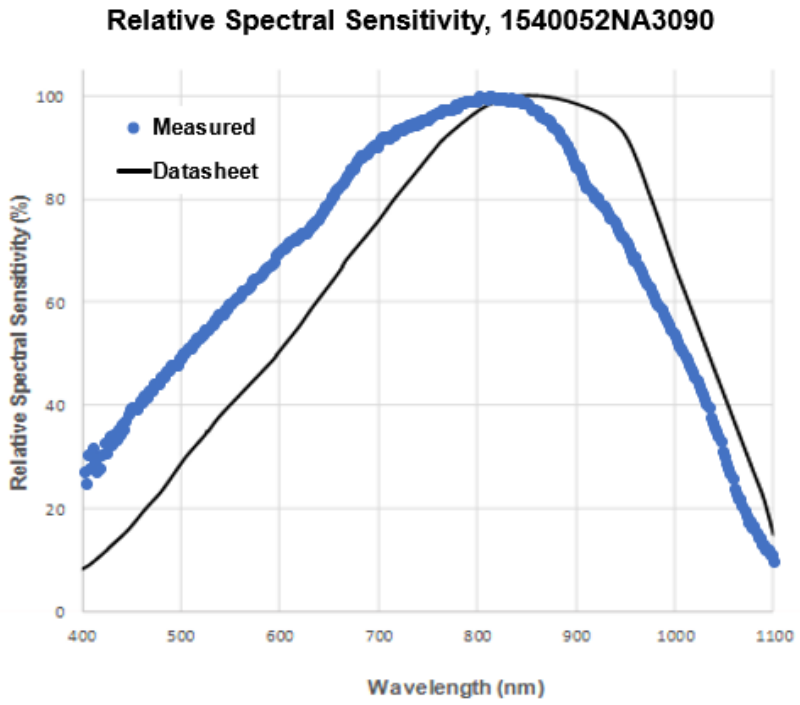


Figure 31. Relative spectral sensitivity of 1540052NA3090 (reproduced from [36]).

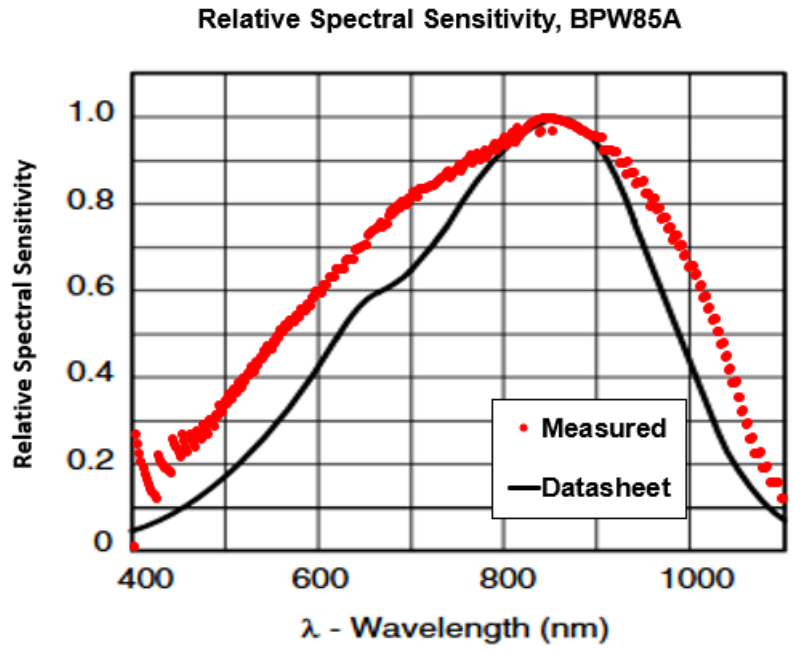


Figure 32. Relative spectral sensitivity of BPW85A (reproduced from [37]).

Both curves are recognizably similar to the ones specified in the datasheets. 1540052NA3090 gives very similar waveform, but there is an offset with the wavelengths of the sensitivity peaks. The datasheet specifies the peak sensitivity to occur at 850 nm, but the measured value for the maximum is 827 nm.

The peak sensitivity for BPW85A is exactly the same for the measured sensitivity and the value in the datasheet, 850 nm. The waveform, however, does not decrease as steeply as the specified curve.

It should be noted that the test conditions for the datasheet values involved optical power density of 0.5 mW/cm$^2$ and a bias voltage of 5 V. These two differences are most likely the most significant source of error in the results, since there is a notable difference in currents with different bias voltages, especially with 1540052NA3090. The I-V characteristic curve also differs under different levels of optical power. The optical power was approximately a thousand times smaller with this setup.

Given the large differences in test conditions, and the low gain in regard to the signal level, the results are encouraging. Major improvement to the setup can be achieved by increasing the optical power output. This can be done by applying a larger bandwidth or a brighter light source, but a better solution might be to use a smaller integrating sphere, or to focus the light beam from the monochromator output directly to the DUT, but also the calibration method should be revised.

The amplifiers themselves can be improved by changing the feedback components to give a more appropriate gain for the specific test case. Ideally most of the output range available should be utilized. The discrepancies in the linearity of the amplifiers, may be solved with debugging, but real-world applications always have unideal properties. All things considered, the results proved the measurement setup and the amplifiers to be functional, and accurate enough to detect even very low signals.

# 7 Conclusions

The goal of this thesis was to construct a measurement setup with an appropriate amplifier for the purposes of photodetector characterization. This goal was achieved by studying optoelectronics and amplifiers, designing testboard PCBs, and assembling the testboards and the measurement equipment into a working system.

The final product is an efficient solution for characterizing photodetector components. Although the new photodetector was not available for characterization, the testboards and the measurement setup were verified to be functional. The measurement setup and the testboards are easily modifiable, and the best amplifier circuit configuration for the specific test can be selected by the user, this makes them suitable for measuring any photodetector. Further improvements to the measurements are achievable by increasing the optical power of incident light, and by readjusting the gain of the amplifiers.

The future of the photodetector development includes also measuring the temperature dependency of the signal and the dark current. Measuring the dark current may be a challenge since it is much smaller than photocurrent, but the results are promising. Detector's speed of response to incident light is also of interest, which will require adjusting the filters of the amplifiers, but this can be done without changing the layout design of the circuit boards.

## References


1 Sze, S. M. Physics of Semiconductor Devices. 2nd edition. New York: Wiley-Interscience publication; 1981.

2 Neamen, Donald A. Semiconductor Physics and Devices: Basic Principles. 3rd edition. New York: McGraw-Hill; 2003.

3 Hu, Chenming. Modern Semiconductor Devices for Integrated Circuits. 1st edition. London: Pearson; 2009.

4 OpenStax. College Physics: OpenStax [Internet]. 2016. p.247. Available from: https://pressbooks.bccampus.ca/collegephysics/chapter/the-pauli-exclusion-principle/ [cited 4 November 2020].

5 Saleh, B.E.A. and Teich, M.C. Fundamentals of Photonics. 2nd edition. New York: Wiley-Interscience publication; 2007.

6 Wilson, J. and Hawkes, J. Optoelectronics: An Introduction. 3rd edition. London: Prentice Hall; 1998.

7 Vishay. TEFD4300F, Silicon PIN Photodiode. Rev 1.3 [Internet]. 2017. Available from: https://www.vishay.com/docs/83472/tefd4300f.pdf [cited 21 December 2020].

8 Vishay. BPV11, Phototransistor [Internet]. 2020. Available from: https://www.vishay.com/docs/81504/bpv11.pdf [cited 21 December 2020].

9 Pcboard. Light Sensitive Resistor (LDR), GL55-series [Internet]. 2020. Available from: https://www.pcboard.ca/ldr-light-dependent-resistor [cited 21 December 2020].

10 Thorlabs. Photodiode Tutorial [Internet]. 2014 Available from: https://www.thorlabs.com/tutorials.cfm?tabID=787382FF-26EB-4A7E-B021-BF65C5BF164B [cited 4 November 2020].

11 Aptechnologies. Photodiode Theory of Operation [Internet]. 2020. Available from: https://www.aptechnologies.co.uk/support/SiPDs/operation [cited 5 November 2020].

12 Industrial-Electronics. Guide to Fiber Optics - Optical drivers and detectors, FIG. 11 Silicon PIN photodiode I-V characteristics [Internet]. 2020. Available from: https://www.industrial-electronics.com/fiber_6.html [cited 21 December 2020].

13 Vishay. Measurement Techniques. Rev 1.4 [Internet]. 2012. Available from: https://www.vishay.com/docs/80085/measurem.pdf [cited 5 November 2020].

14 Technical University of Lodz. Measurement of photodetectors [Internet]. 2013. Available from: http://www.dsod.p.lodz.pl/materials/OPT10_IFE.pdf [cited 9 November 2020].

15 Electronics-notes. Light Dependent Resistor LDR: Photoresistor [Internet]. 2020. Available from: https://www.electronics-notes.com/articles/electronic_components/resistors/light-dependent-resistor-ldr.php [cited 12 November 2020]

16 Osram. Product datasheet 64657 HLX [Internet]. 2020. Available from: https://www.osram.com/appsj/pdc/pdf.do?cid=GPS01_1028526&vid=PP_EUROPE_Europe_eCat&lid=EN&mpid=ZMP_56130 [cited 27 December 2020].

17 Shimadzu. Characteristics of Single and Double Monochromator UV-VIS Spectrophotometers, Fig. 1 Principles of Monochromators [Internet]. 2020. Available from: https://www.shimadzu.com/an/service-support/technical-support/analysis-basics/fundamentals-uv/single_double.html [cited 21 December 2020].

18 Bentham. TMc300 Single Monochromator, Overview [Internet]. 2020. Available from: https://www.bentham.co.uk/products/components/monochromators/configurable-monochromators/tmc300-single-monochromator-38/ [cited 21 December 2020]

19 Thorlabs. Compact USB Power Meter with Silicon Photodiode Detector, PM16-120 [Internet]. 2015. Available from:PM16-120 https://www.thorlabs.com/drawings/9765355c97b2db3e-06136612-B01C-940A-06EBB65C899B185F/PM16-120-SpecSheet.pdf [cited 4 January 2021].

20 National Instruments. NI 9215 Datasheet [Internet]. 2016. Available from: https://www.ni.com/pdf/manuals/373779a_02.pdf [cited 4 January 2021].

21 National Instruments. NI 9263 Datasheet [Internet]. 2016. Available from: https://www.ni.com/pdf/manuals/373781b_02.pdf [cited 4 January 2021].

22 Thorlabs. 30 and 60 mm Cage System Construction Rods, Engraved 6 inch ER Rods with 60 mm Cage Plates [Internet]. 2020. Available from: https://www.thorlabs.com/newgrouppage9.cfm?objectgroup_id=4125 [cited 21 December 2020].

23 Silvonen, K. Elektroniikka ja puolijohdekomponentit. Helsinki: Otatieto; 2009.

24 Hahn, A. Application of Rail-to-Rail Operational Amplifiers [Internet]. 1999. Available from: https://www.ti.com/lit/an/sloa039a/sloa039a.pdf [cited 13 November 2020].

25 Mancini, R. Op amp stability and input capacitance [Internet]. 2004. Available from: https://www.ti.com/lit/an/slyt087/slyt087.pdf [cited 16 November 2020].

26 Carter, B. and Brown, T. Handbook of operational amplifier applications [Internet]. 2016. Available from: https://www.ti.com/lit/an/sboa092b/sboa092b.pdf [cited 16 November 2020].

27 Baker, B. How to Design Stable Transimpedance Amplifiers for Automotive and Medical Systems [Internet]. 2017. Available from: https://www.digikey.fi/fi/articles/how-to-design-stable-transimpedance-amplifiers-automotive-medical-systems [cited 18 November 2020].

28 Texas Instruments. Simplifying Current Sensing: How to design with current sense amplifiers [Internet]. 2020. Available from: https://www.ti.com/lit/eb/slyy154a/slyy154a.pdf [cited 19 November 2020].

29 Linear Technology. LTC6268/LTC6269, 500MHz Ultra-Low Bias Current FET Input Op Amp [Internet]. Available from: https://www.analog.com/media/en/technical-documentation/data-sheets/62689f.pdftlv9051 [cited 23 November 2020].

30 Texas Instruments. TLV9051/ TLV9052/ TLV90545-MHz,15-V/µs High Slew-Rate, RRIO Op Amp [Internet]. 2019. Available from: https://www.ti.com/lit/ds/symlink/tlv9052.pdf [cited 23 November 2020].

31 Microchip. MCP1702, 250 mA Low Quiescent Current LDO Regulator [Internet]. 2010. Available from: https://ww1.microchip.com/downloads/en/DeviceDoc/22008E.pdf [cited 24 November 2020].

32 Maxim. MAX6100–MAX6107, Low-Cost, Micropower, Low-Dropout, High-Output-Current, SOT23 Voltage References [Internet]. 2002. Available from: https://datasheets.maximintegrated.com/en/ds/MAX6100-MAX6107.pdf [cited 24 November 2020].

33 TDK. NTC thermistors for temperature measurement Current, B57164K [Internet]. 2013. Available from: http://www.farnell.com/datasheets/2006215.pdf [cited 15 December 2020].

34 SMC Diode Solutions. SMDA03C-4-2 THRU SMDA 24C-4-2 TVS ARRAY SERIES. Rev. A [Internet]. Available from: http://www.smc-diodes.com/propdf/SMDA03C-4-2%20THRU%20SMDA24C-4-2%20N0299%20REV.A.pdf [cited 3 November 2020].

35 Luna Optoelectronics. Plastic Photodiode Package with Leads, PDB-C142. Rev. 01-04-16 [Internet]. 2016. Available from: https://media.digi-key.com/pdf/Data%20Sheets/Photonic%20Detetectors%20Inc%20PDFs/PDB-C142.pdf [cited 12 January 2021].

36 Würth Elektronik. WL-TTRW THT Phototransistor Round Waterclear, 1540052NA3090. Rev. 1 [Internet]. 2019. Available from: https://www.mouser.fi/datasheet/2/445/1540052NA3090-1838921.pdf [cited 11 January 2021].

37 Vishay. BPW85, Silicon NPN Phototransistor. Rev. 2.1 [Internet]. 2014. Available from: https://www.vishay.com/docs/81531/bpw85a.pdf [cited 11 January 2021].

# Appendix 1: Mainboard Schematic – Sheet 1 of 2

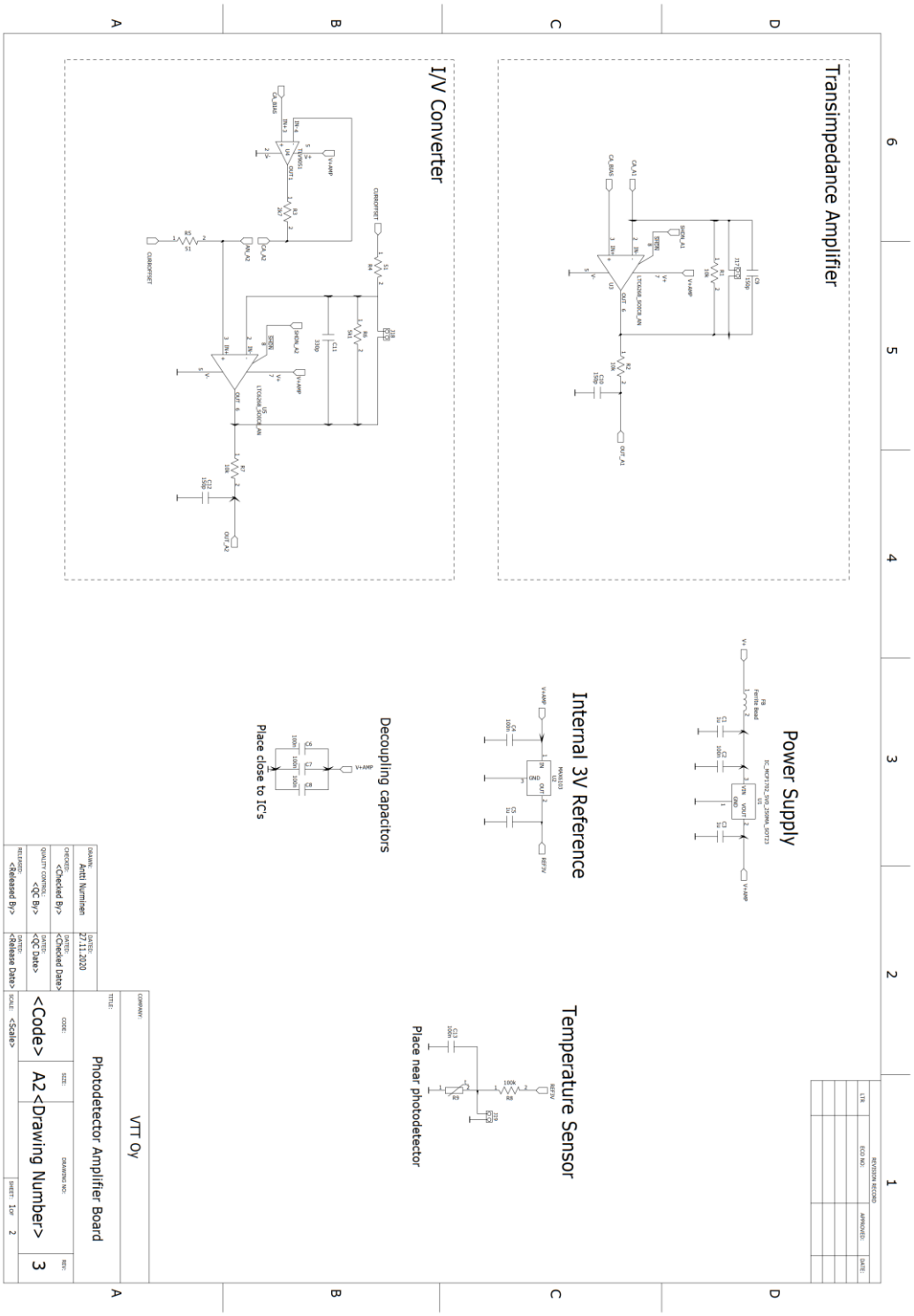

## Appendix 1: Mainboard Schematic – Sheet 2 of 2

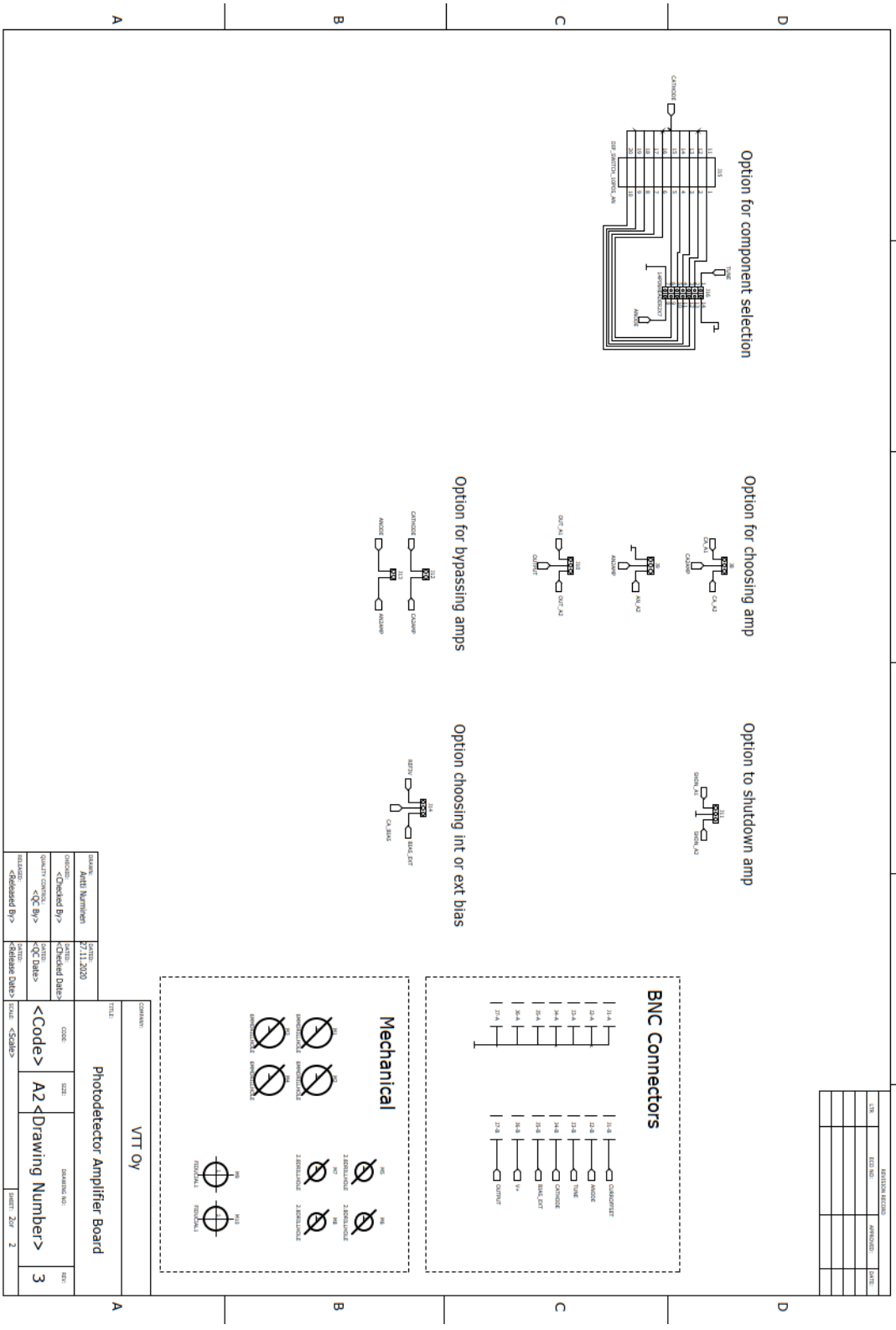

## Appendix 2: Mainboard Layout

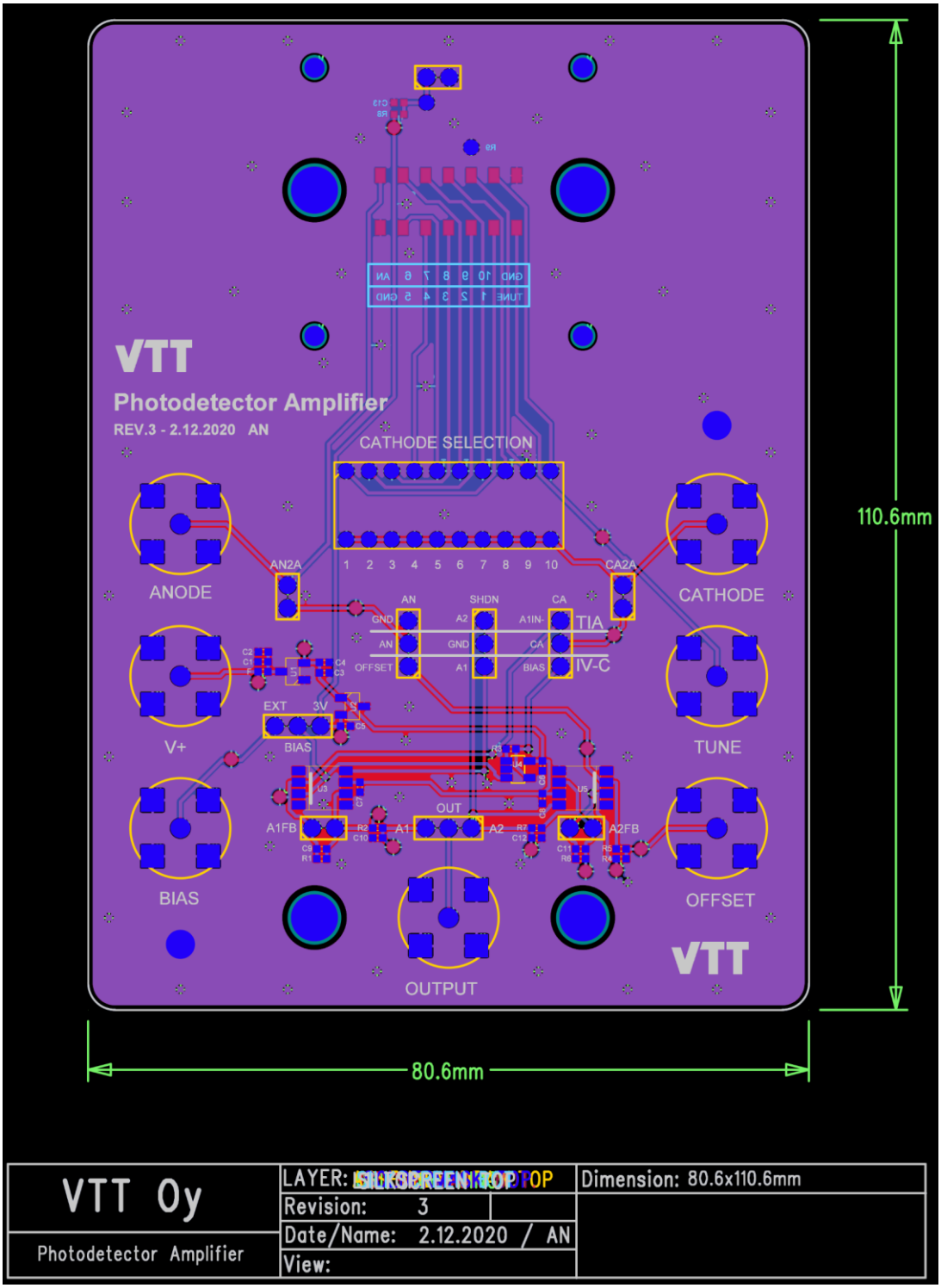

## Appendix 3: Daughterboard Schematic

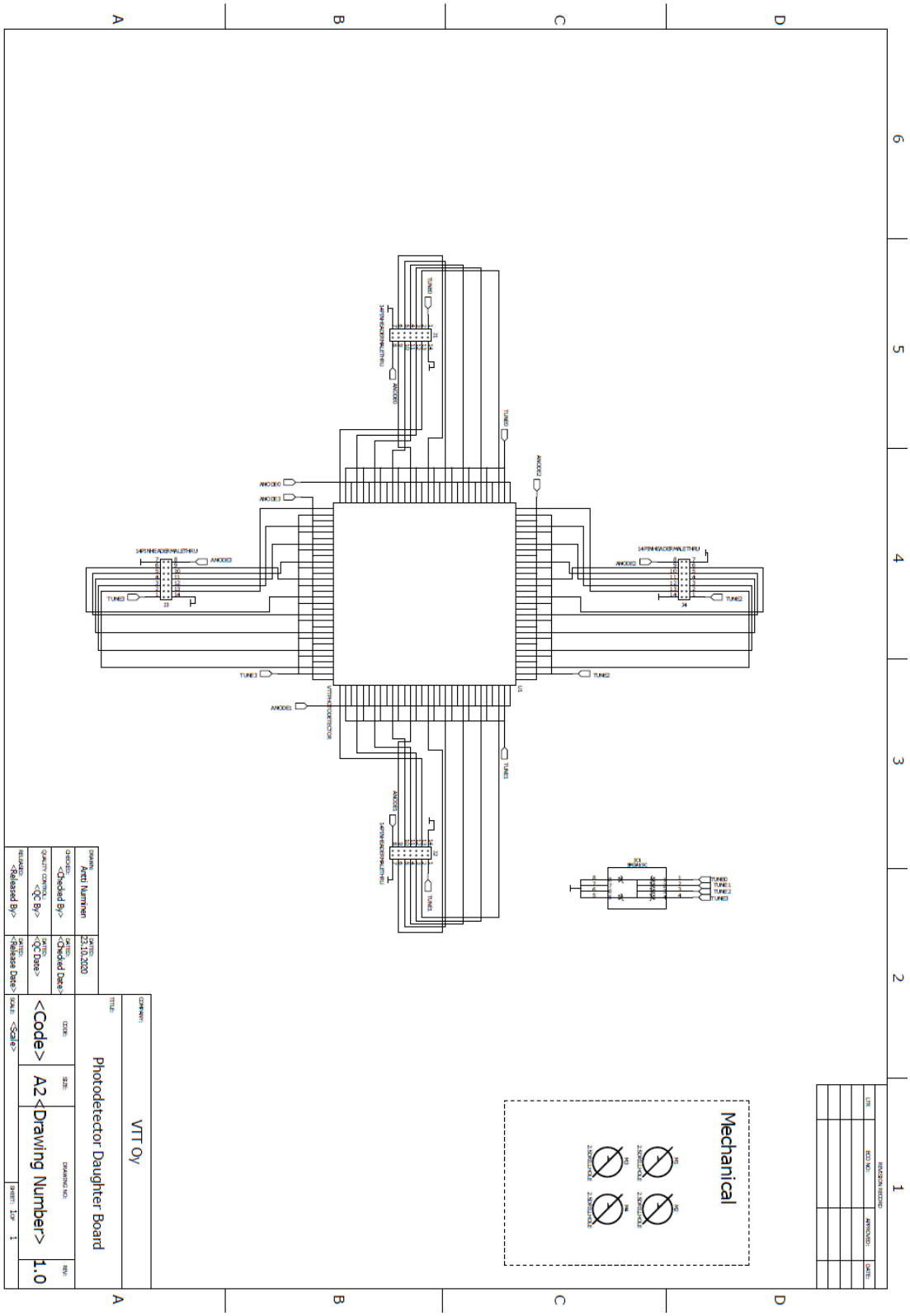

## Appendix 4: Daughterboard Layout